TG 1073
JULY 1969
Copy No. 17

AD696063

Technical Memorandum

THERMAL STRESSES IN OGIVAL RADOMES WITH TEMPERATURE-DEPENDENT MATERIAL PROPERTIES

by M. B. TATE

DDC
RECEIVED
NOV 6 1969

THE JOHNS HOPKINS UNIVERSITY • APPLIED PHYSICS LABORATORY

This document has been approved for public release and sale; its distribution is unlimited.

Reproduced by the
CLEARINGHOUSE
for Federal Scientific & Technical
Information Springfield Va. 22151

58

TG 1073

JULY 1969

Technical Memorandum

THERMAL STRESSES IN OGIVAL RADOMES WITH TEMPERATURE-DEPENDENT MATERIAL PROPERTIES

by M. B. TATE

THE JOHNS HOPKINS UNIVERSITY • APPLIED PHYSICS LABORATORY
8621 Georgia Avenue, Silver Spring, Maryland 20910

Operating under Contract NOw 62-0604-c with the Department of the Navy

This document has been approved for public release and sale; its distribution is unlimited.

THE JOHNS HOPKINS UNIVERSITY
APPLIED PHYSICS LABORATORY
SILVER SPRING MARYLAND

ABSTRACT

The solution that is developed herein can be used to compute thermal stresses and displacements in the moderately thick walls of appreciably curved ogival radome shells whose material properties change with heat intensity along the span and through the wall. No restriction is placed on temperature dependent variations of the thermal strain expression.

A restriction imposed on the theory is that the wall material must not be overstrained. Overstrain is any amoun beyond the elastic limit in excess of allowable strain that accompanies a maximum stress equal to the usable strength of the material as determined for the worst heating condition in a given application.

Three examples of the computerized results are presented. The first example deals with a 28.3" x 6.75" bicentric-ogive radome; the second, with a thick-walled hemispherical radome; and the third, with a thin-walled hemisphere. In these calculations, linear spanwise temperature distributions are used that were obtained from experimental and heat-transfer analyses of a radome tested in a wind tunnel. Through the wall, over specified layers, the thermal-strain function is approximated as being linear with temperature. However, the temperature varies as a third-order nonlinear function through the thickness of the wall as found for the test radome. It appears that errors due to the approximation amount to less than four percent in general.

It was found that stresses in the bicentric-ogive radome were within safe limits in regard to strengths of the wall material. Good agreement was obtained between computed and experimentally determined stresses at the one point, 1.75 inches behind the tip, where strains were measured. Analyzed for comparison, the thick-walled hemispherical radome was overstressed, but the thin-walled hemisphere was sufficiently strong.

It is also concluded that additional information is needed on temperature distributions, nosecap behavior, thermal stress maxima, and the effects of radome-missile joints.

THE JOHNS HOPKINS UNIVERSITY
APPLIED PHYSICS LABORATORY
SILVER SPRING MARYLAND

TABLE OF CONTENTS

LIST OF ILLUSTRATIONS

THE JOHNS HOPKINS UNIVERSITY
APPLIED PHYSICS LABORATORY
SILVER SPRING MARYLAND

I. INTRODUCTION

In his famous treatise on elasticity, A. E. H. Love [1][1] discussed the analysis of appreciably curved and moderately thick-walled shells. He then proceeded with examples in which he made certain approximations that let him neglect terms found to be unimportant within the range of consideration. Many authors thereafter adopted Love's approximations and developed the modern thin-shell theory, [2], [3], [4], and [5], for example.

Today's requirements for heat-resistant structures of comparatively thick-walled shell construction have led to further investigation of the problem. McDowell and Sternberg [6] examined spherical shells, and several writers studied cylindrical shells: Tsao [7], Lee [10], Hoff and Madsen [11], Rivello [12] and [16], and Bijlaard, Dohrmann and Duke [18]. Conical shells were analyzed by Lu and Chang [14] and Weiss [17]. Buckling effects, moreover, were included in [11] and [14], and sandwich constructions were discussed in [12] and [16].

Thermal stresses in beams were computed by Barrekette [8], and radome materials for high temperature usage were compared by Weckesser, Hallendorff and Suess [15]. The stiffness-matrix method was employed by Dailey [13] to obtain numerical solutions.

In [9], F. Lane derived solutions for shells of revolution, and D. E. Magnus and D. Eisen presented digital-computer programs for numerical evaluations. Lane used variational calculus to minimize the strain energy of a shell to obtain his results.

Numerical and theoretical analyses developed in the ensuing text require that the radome wall material must not be overstrained. Overstrain refers to a strain that exceeds the elastic limit at a concurrent temperature. Reports [19] to [27], inclusive, were prepared as part of the overall thermal-stress investigation.

[1] Numerals in brackets denote references listed at the end of this report.

II. ACKNOWLEDGEMENTS

The writer fully appreciates many helpful suggestions offered by Mr. W. C. Caywood and his keen interest in reading the several reports on this investigation. Also, the assistance of Mr. R. L. McCutcheon and his coworkers, who programmed the computer solutions, is gratefully acknowledged.

III. NOMENCLATURE

A,B,C:	Constants of integration
D:	Wall stiffness factor, $D = Eh^3/12(1-\nu^2)$
E:	Young's modulus of elasticity, psi
F:	Force; Function; Fahrenheit
H:	Intercept height, inches
I:	Wall moment of inertia, $I = h^3/12$
J,K:	Constants
L:	An operator
M:	Moment resultant, ippi
N:	Normal-stress resultant, ppi
P:	Function
Q:	Shear-stress resultant, ppi
R:	Spatial radius, inches
S:	A series or its sum
T:	Temperature, °F
V:	Wall-slope change, radians
W:	Function
Y:	Variable
Z:	Geometric axis of radome
a,b:	Series coefficients
c:	Half thickness of wall (c=h/2), inches
e:	Normal strain, ipi
f:	Function
h:	Wall thickness, inches
i:	Positive integer; 1,2,3,...
k:	Constant
ℓ:	Length, inches
m,n:	Positive integers; 1,2,3,...
p:	Function; Pressure, psi
q:	Auxiliary shear function, ppi
r:	Planar radius, inches
s:	A series or its sum
u,w:	Displacement functions, inches
x:	Thickness variable ratio, x = y/c
y:	Thickness coordinate, inches
z:	Coordinate along geometric axis, inches
β:	Wall bending parameter, radians
ϵ:	Normal strain, ipi
θ:	Coordinate angle of rotation, degrees or radians
ν:	Poisson's ratio
σ	Normal stress, psi
τ:	Shear stress, psi
χ:	Curvature change, radians per inch
ψ:	Coordinate angle of azimuth, degrees or radians

The following symbols are used as subscripts:

a:	Anterior or outer surface of wall
b:	Base of radome at the body of a missile
c:	Central surface of wall
g:	General

i,m,n:	Indices
o:	Origin or initial value (zero)
p:	Particular
q:	Referred to function q
s:	Secondary or inner surface of wall
t:	Thermal or temperature
y:	In the y direction
r,θ,z:	Cylindrical-coordinate directions
R,θ,ψ:	Spherical-coordinate directions

IV. THERMAL STRESS EXPRESSIONS

1. RADOME WALL STRESSES

When the radome mainbody is an ogival segment, such as the one illustrated in Figure 1a, meridian (σ_ψ) and hoop (σ_θ) stresses can be determined with a computer program based on the following equations.

$$\sigma_\psi = \sigma_a - \sigma_t, \qquad \sigma_\theta = \sigma_b - \sigma_t \tag{1}$$

In the foregoing expressions, σ_t represents a function having the dimensions of stress (psi) given by

$$\sigma_t = E\epsilon_t/(1-\nu) \tag{2}$$

and σ_a and σ_b were calculated from the equations written below.

$$\sigma_a = \frac{R_c\sigma_1}{R} - \frac{\nu yH(\sigma_2 - \nu\sigma_1)}{(1-\nu^2)rR}, \qquad \sigma_b = \frac{R_c\sigma_2}{R} - \frac{yH(\sigma_2 - \nu\sigma_1)}{(1-\nu^2)rR} \tag{3}$$

$$\sigma_1 = \frac{N_1}{h} + \frac{M_1 y}{I}, \qquad \sigma_2 = \frac{N_2}{h} + \frac{M_2 y}{I} \tag{4}$$

Dimensions h, H, R_c and variables y, r, R are defined on Figure 1a, which shows the wall profile of the radome. Symbol "I" denotes moment of inertia per unit length of a section of the wall ($I = h^3/12$). And ν is Poisson's ratio while normal stress (N_i) and moment (M_i) resultants are described in the next article.

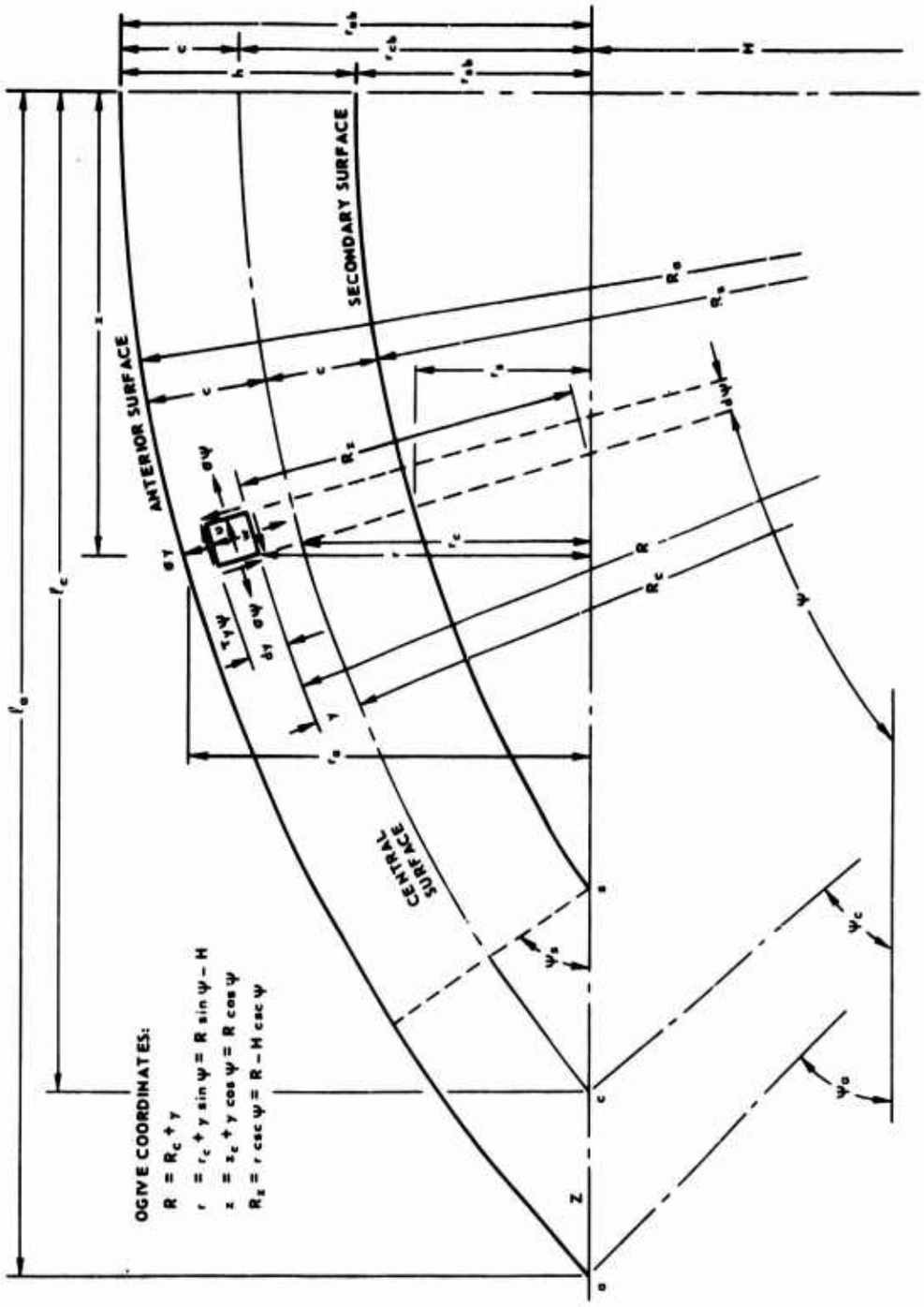

Fig. 1a OGIVAL RADOME WALL DIMENSIONS

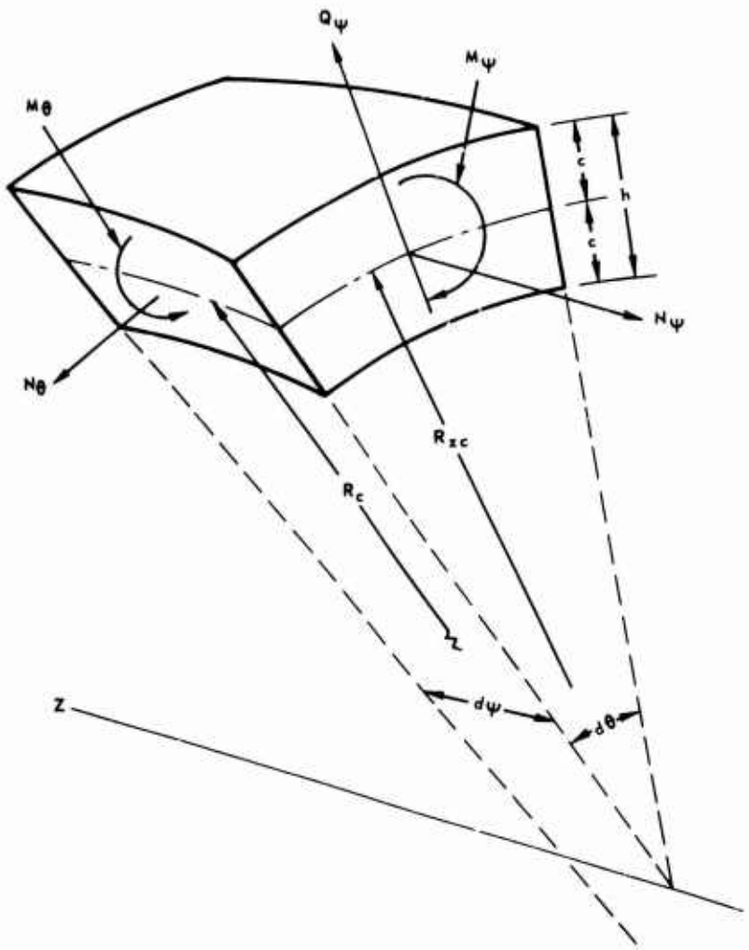

Fig. 1b RADOME-WALL ELEMENT WITH STRESS RESULTANTS AND BENDING MOMENTS

2. STRESS AND MOMENT RESULTANTS

Two normal stress resultants (N_1 and N_2) appear in equations (4). By definition, they are

$$N_1 = N_\psi + N_{t\psi}, \qquad N_2 = N_\theta + N_{t\theta} \tag{5}$$

where all four of the right-hand terms are obtained from the following integrals.

$$N_\psi = \int_{-c}^{+c} \frac{r\sigma_\psi}{r_c}\, dy, \qquad N_\theta = \int_{-c}^{+c} \frac{R\sigma_\theta}{R_c}\, dy \tag{6}$$

$$N_{t\psi} = \int_{-c}^{+c} \frac{r\sigma_t}{r_c}\, dy, \qquad N_{t\theta} = \int_{-c}^{+c} \frac{R\sigma_t}{R_c}\, dy \tag{7}$$

Furthermore, the shearing stress resultant (Figures 1b and 2)

$$Q_\psi = \int_{-c}^{+c} \frac{r\tau_{y\psi}}{r_c}\, dy \tag{8}$$

is closely related to the first two, equations (6), as discussed in Appendices A, C, D, G, and References [24], [26], and [27].

Moments that bend the wall of the radome occur in equations (4) as M_1 and M_2. They are defined to be

$$M_1 = M_\psi + M_{t\psi}, \qquad M_2 = M_\theta + M_{t\theta} \tag{9}$$

where the four right-hand terms are calculated with integrals that are written below. (Also, see Figure 1b).

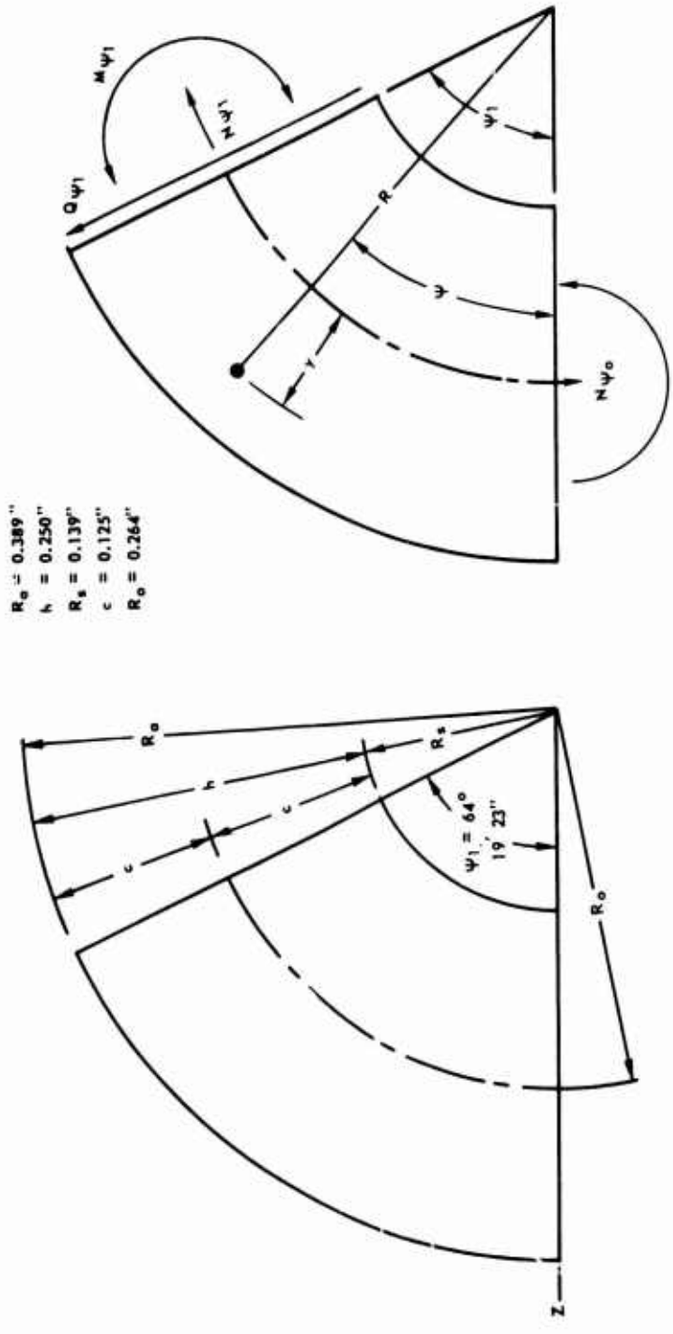

Fig. 2 NOSECAP DIMENSIONS AND RESULTANTS

$$M_{\psi} = \int_{-c}^{+c} \frac{r\sigma_{\psi}}{r_c} ydy, \qquad M_{\theta} = \int_{-c}^{+c} \frac{R\sigma_{\theta}}{R_c} ydy \tag{10}$$

$$M_{t\psi} = \int_{-c}^{+c} \frac{r\sigma_t}{r_c} ydy, \qquad M_{t\theta} = \int_{-c}^{+c} \frac{R\sigma_t}{R_c} ydy \tag{11}$$

The preceding functions are evaluated from relationships that are presented in the appendices and in References [19] to [27], inclusive. Outer surface temperatures are shown in Figure 3.

3. SOLUTIONS

(a) General Solutions - For numerical work, it is frequently expedient to restrict the expansion interval of infinite series that are employed in general solutions. This was done in the example of Part VI-1 wherein three intervals span the length of the radome. The nosecap lies within $0 \leq \psi \leq \psi_1 = 64°19'23"$: (Figure 2), and the mainbody (Figure 1) is composed of two segments (MB1 and MB2) whose defining intervals are

$$64°19'23" = \psi_1 \leq \psi \leq \psi_3 = 73°44'23" \qquad \text{(for MB1)}$$

$$73°44'23" = \psi_3 \leq \psi \leq \psi_b = 90° \qquad \text{(for MB2)}$$

where 90° coincides with the radome base at which point it is attached to the cylindrical body of a missile.

For general solutions, infinite series are of the forms

$$s_m = \sum_{n=o}^{\infty} a_{mn} Y^n, \qquad S_m = \sum_{n=o}^{\infty} n a_{mn} Y^{n-1} \tag{12}$$

with numerical results discussed in the appendices, and the variable Y is shown below for MB1 and MB2.

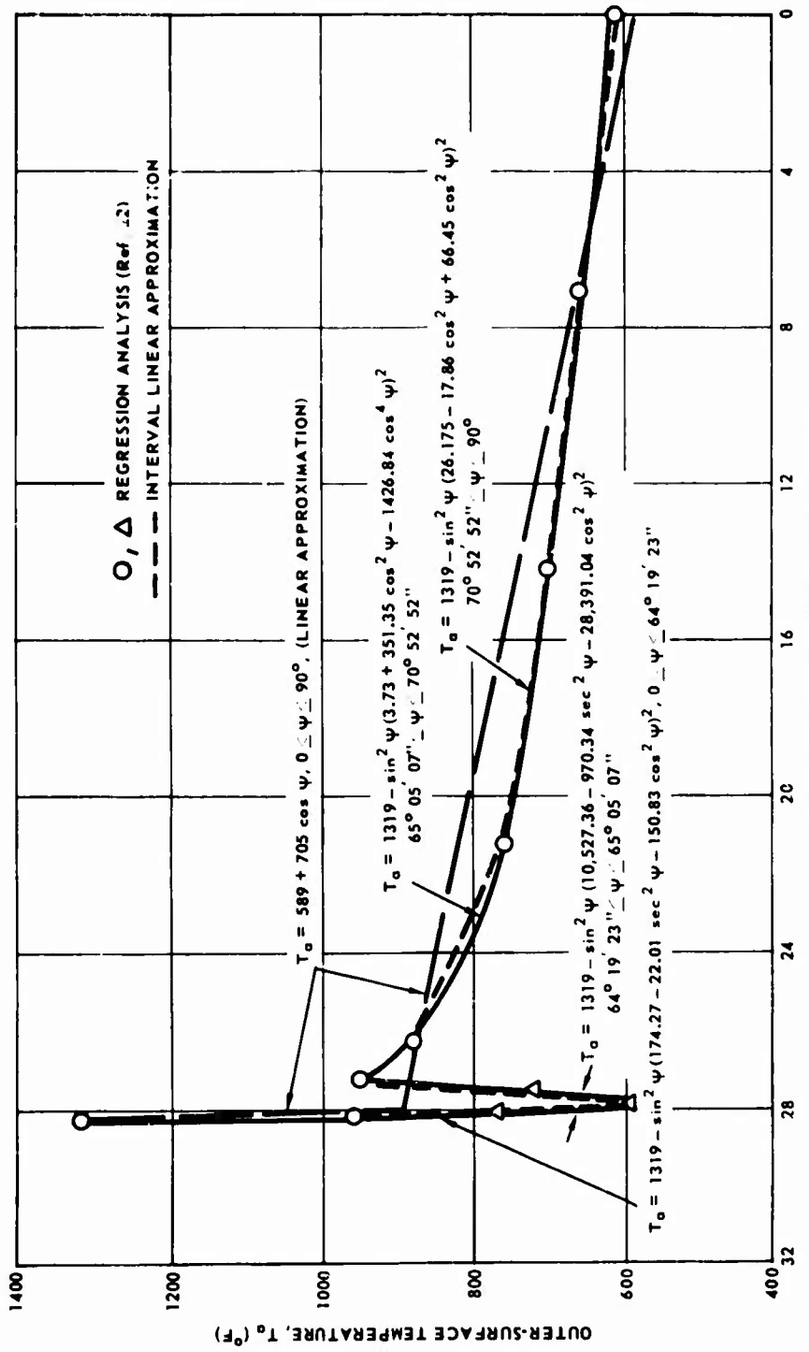

Fig. 3 SPANWISE TEMPERATURE DISTRIBUTION FOR BICENTRIC-OGIVE RADOME

$$Y = \frac{\sin \psi - \sin \psi_2}{\sin \psi_2 - \sin \psi_1}, \qquad \psi_1 \le \psi \le \psi_3 \tag{13}$$

$$Y = \frac{\sin \psi - \sin \psi_4}{\sin \psi_4 - \sin \psi_3}, \qquad \psi_3 \le \psi \le 90^\circ \tag{14}$$

From both expressions (13) and (14), values are within $-1 \le Y \le +1$ from left to right ends of each interval. Subsequently (Appendix D), it is demonstrated that the general solution is

$$N_{\psi g} = \cos \psi \sum_{m=1}^{4} B_m f_m(\psi) \qquad N_{\theta g} = N_{\psi g} + \frac{r_c}{R_c} \sum_{m=1}^{4} B_m F_m(\psi) \tag{15}$$

where the B_m ($m = 1,2,3,4$) are constants of integration determined by boundary conditions as explained in Appendix E.

The functions f_m, F_m depend on s_m, S_m being computed with

$$f_m(\psi)_{m=1,2} = s_m, \qquad f_m(\psi)_{m=3,4} = s_m \cos \psi \tag{16}$$

$$F_m(\psi)_{m=1,2} = k_i S_m \cos \psi, \qquad F_m(\psi)_{m=3,4} = k_i S_m \cos^2 \psi - S_m \sin \psi \tag{17}$$

wherein k_i represents k_1 in MB1 and k_2 in MB2 as shown below in equations (18).

$$k_1 = \frac{1}{\sin \psi_2 - \sin \psi_1}, \qquad k_2 = \frac{1}{\sin \psi_4 - \sin \psi_3} \tag{18}$$

The bending moments are calculated from changes in curvature of the wall of the radome with orthogonal components expressed by

$$\chi_\psi = \frac{1}{R_c} \frac{dV}{d\psi}, \qquad \chi_\theta = \frac{V \cos \psi}{r_c} \tag{19}$$

where V denotes change of slope of the radome wall induced by thermoelastic effects. The moments are

$$M_1 = -D(\chi_\psi + \nu\chi_\theta), \qquad M_2 = -D(\nu\chi_\psi + \chi_\theta) \tag{20}$$

$$D = EI/(1-\nu^2) = Eh^3/12(1-\nu^2) \tag{21}$$

and the curvature changes are calculated from the next two equations.

$$\chi_{\theta g} = \frac{\cos\psi}{R_c} \sum_{m=1}^{4} B'_m f_m(\psi), \qquad \chi_{\psi g} = \chi_{\theta g} + \frac{r_c}{R_c^2} \sum_{m=1}^{4} B'_m F_m(\psi) \tag{22}$$

The preceding functions, constants B_m and B'_m, and computation of series coefficients a_{mn} in equations (12) by means of recurrence formulas are described in greater detail in the appendices and in Reference [26].

(b) Particular Solutions - In general, particular solutions cannot be obtained in closed form to compute stress and moment resultants in the mainbody (Figure 1). It is demonstrated in Appendix D, however, that approximate formulas can be developed that describe the desired functions within about one-half percent. The approximation functions are

$$q_p = B_5 + \frac{r_c B_8}{R_c} + \frac{R_c(B_7 + B_8\cos\psi)}{r_c\tan\psi}, \qquad Q_\psi = \frac{qR_c\sin\psi}{r_c}, \qquad N_\psi = Q_\psi\cot\psi \tag{23}$$

$$N_{\theta p} = \left[B_5 - \frac{R_c B_8}{r_c}\right]\cos\psi - \frac{R_c}{r_c}\left[\csc^2\psi + \frac{R_c\cos\psi}{r_c\tan\psi}\right](B_7 + B_3\cos\psi) \tag{24}$$

$$V_p = B'_5 - \frac{r_c B'_8}{R_c} - \frac{R_c(B'_7 + B'_8\cos\psi)}{r_c\tan\psi}, \qquad \chi_\theta = \frac{V\cos\psi}{r_c} \tag{25}$$

$$\chi_{\psi p} = \left[\frac{B'_8}{r_c} - \frac{B'_6}{R_c}\right]\cos\psi + \frac{1}{r_c}\left[\csc^2\psi + \frac{R_c\cos\psi}{r_c\tan\psi}\right](B'_7 + B'_8\cos\psi) \tag{26}$$

in which q is an auxiliary shear function used to find the total shear (Q_ψ) by means of equation (23). Integration constants B_m and B'_m are calculated in Appendix D from temperature relationships, and they are fully developed in Reference [24].

V. THERMOELASTIC DISPLACEMENTS

1. WALL EXTENSION

In Appendix F, the wall-extension component (w) of displacement is developed as

$$w = w_i \sin \psi + w_q - w_t \tag{27}$$

where w_i is a constant of integration (equalling w_1 in MB1 and w_2 in MB2), w_q is a function that depends on the auxiliary shear function (q), equations (100) and (101), and w_t depends on the temperature distribution as given by equations (29), (30), and (31).

2. RADIAL DISPLACEMENT

After finding w from equation (27), the radial component of displacement (u) is calculated with

$$u = r_c \csc \psi (N_2 - \nu N_1)/Eh - w \cot \psi \tag{28}$$

where the coordinates are shown in Figures 1a and 1b, and the other terms are as defined previously. This relation for u is obtained in Appendix F.

VI. EXPERIMENTAL DATA AND HEAT TRANSFER ANALYSES

1. TEMPERATURE DATA

(a) Wall-Thickness Distributions - Available information on radome temperature distributions were analyzed and reported in Reference [22]. Temperature distributions that are shown in Figure 4 were developed in the referenced investigation together with References [20] and [21].

(b) Spanwise Distributions - The spanwise temperature distributions found in Reference [22] along the outer, central, and inner surfaces of the test radome are plotted in Figure 5. They are based on the general relationships developed in Reference [20], and the coefficients are empirical.

(c) Temperature-Distribution Function - With but slight error, it was found in Reference [22] that the approximate temperature distribution throughout the wall of the radome was

$$T = T_a f(x) \tag{29}$$

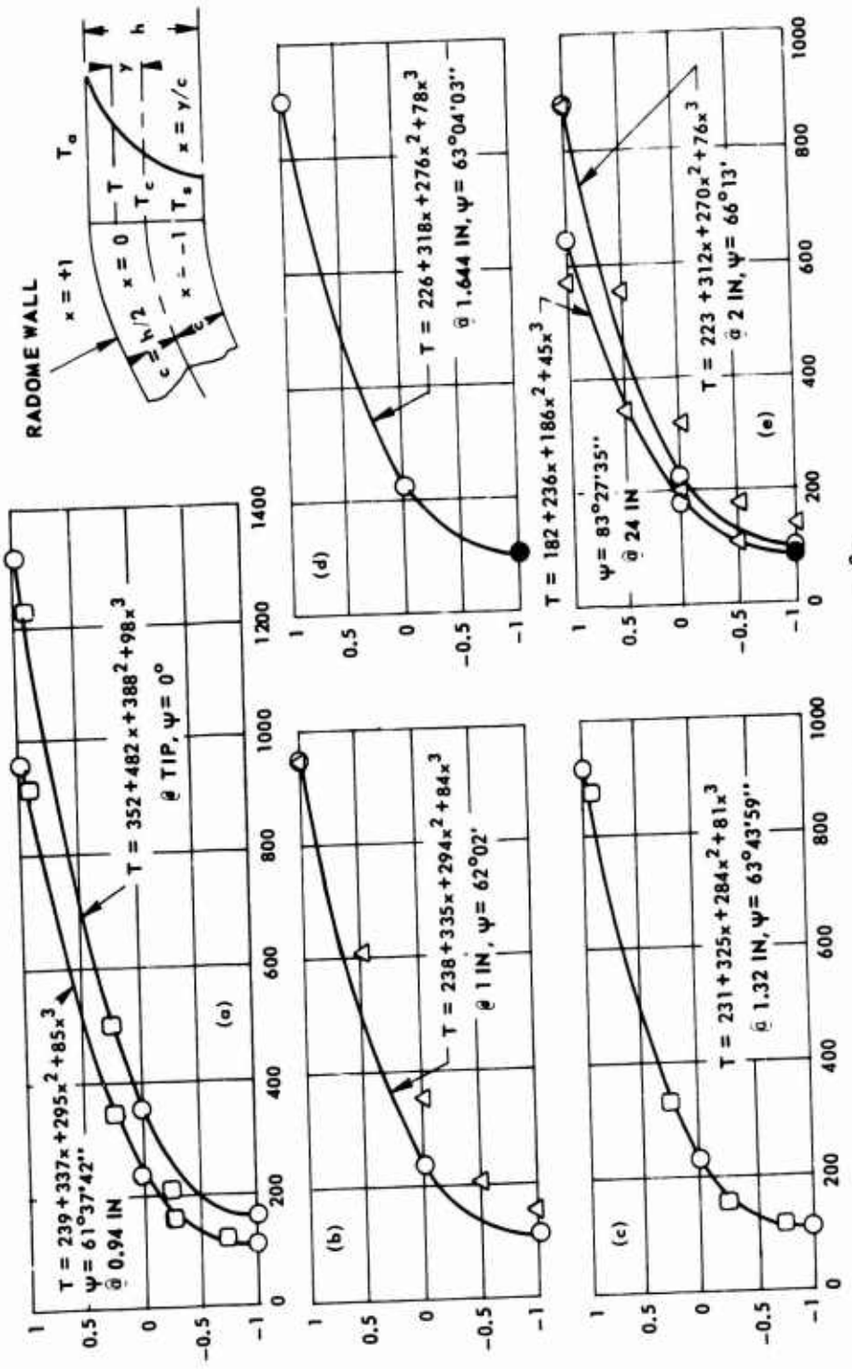

Fig. 4 WALL THICKNESS DISTRIBUTIONS OF TEMPERATURE FOR 28.3-INCH x 6.75-INCH ·'ON KARMAN RADOME

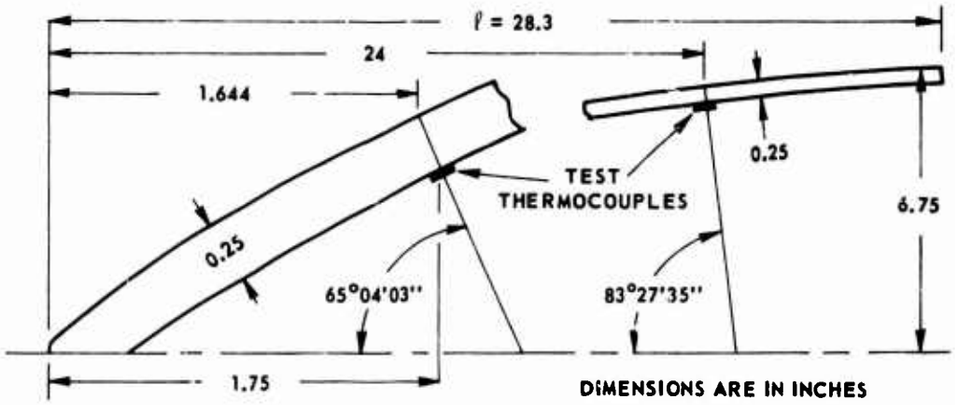

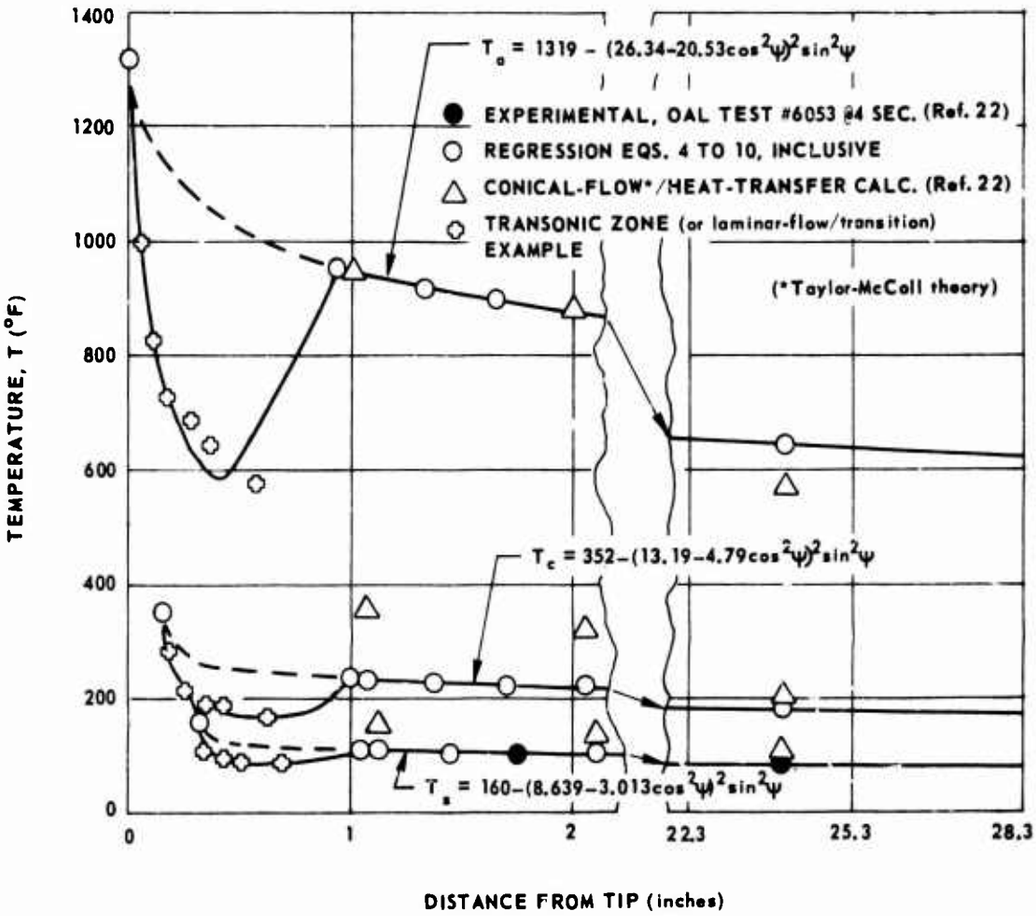

Fig. 5 EXTERIOR, CENTRAL, AND INTERIOR SURFACE SPANWISE TEMPERATURE DISTRIBUTIONS FOR 28.3-INCH x 6.75-INCH VON KARMAN TEST RADOME

where $T = T(\psi,y)$ is a separable function of ψ and $x = y/c$, with y being the wall thickness variable and ψ the coordinate angle as in Figure 1a. For thickness variation, we have

$$f(x) = \sum_{n=o}^{3} f_n x^n = 0.257 + 0.358\ x + 0.305\ x^2 + 0.084\ x^3 \qquad (30)$$

in which numerical values of coefficients (f_n) are stated in the expanded form on the right.

The exterior-surface temperature distribution is given by

$$T_a = T_a(\psi) \qquad (31)$$

which is shown in Figure 3 for the bicentric-ogive radome of the first example in Part VIII.

2. STRENGTH DATA

(a) Strain Measurements - Strains were measured along the inner surface of the wall at 1.75 inches from the tip of the radome employed in the wind tunnel tests reported in References [21] and [22]. No breakage was reported for test results used in analysis.

(b) Stress Results - Stresses were calculated from the strain measurements. As a point of comparison, an experimentally determined meridian stress of 18,000 psi was found at the inner wall surface at 1.75 inches from the tip of the test radome.

VII. NOSECAP AS A SPHERICAL SEGMENT

1. WALL STRESSES

Frequently, a radome nosecap is the spherical segment of a half-caliber ogive pictured by Figure 2. In such cases, formulas (3) reduce to

$$\sigma_a = R_o\sigma_1/R, \qquad \sigma_b = R_o\sigma_2/R \qquad (32)$$

and the other relations are unchanged. Radius R_o is the principal radius of curvature of the central surface, which is shown in Figure 2 also.

2. STRESS AND MOMENT RESULTANTS

The normal stress resultants (N_1 and N_2) that appear in equations (4) are given by

$$N_1 = N_\psi + N_t, \qquad N_2 = N_\theta + N_t \tag{33}$$

where the right-hand terms are obtained from the following integrals.

$$N_\psi = \int_{-c}^{+c} \frac{R\sigma_\psi}{R_o}\, dy, \qquad N_\theta = \int_{-c}^{+c} \frac{R\sigma_\theta}{R_o}\, dy \tag{34}$$

$$N_t = N_{t\psi} = N_{t\theta} = \int_{-c}^{+c} \frac{R\sigma_t}{R_o}\, dy \tag{35}$$

Also, the wall bending moments (M_1 and M_2) that occur in equations (4) are defined to be

$$M_1 = M_\psi + M_t, \qquad M_2 = M_\theta + M_t \tag{36}$$

where the right-hand terms are computed with the integrals shown below.

$$M_\psi = \int_{-c}^{+c} \frac{R\sigma_\psi}{R_o}\, ydy, \qquad M_\theta = \int_{-c}^{+c} \frac{R\sigma_\theta}{R_o}\, ydy \tag{37}$$

$$M_t = M_{t\psi} = M_{t\theta} = \int_{-c}^{+c} \frac{R\sigma_t}{R_o}\, ydy \tag{38}$$

The preceding functions are evaluated from relationships that are presented in the appendices, and outer surface temperatures are shown in Figure 3.

3. SOLUTIONS

(a) General Solutions - For the nosecap, whose interval is shown in Figure 2 as

$$0 \le \psi \le \psi_1 = 64°19'23"$$

the general solutions corresponding to series (12) are obtained with variable Y replaced by 1-cos ψ; e.g.,

$$s_m = \sum_{n=o}^{\infty} b_{mn}(1-\cos\psi)^n, \qquad S_m = \sum_{n=o}^{\infty} nb_{mn}(1-\cos\psi)^n \tag{39}$$

and the normal stress resultants are given by the following two equations.

$$N_{\psi g} = \cos\psi \sum_{m=1}^{4} A_m s_m, \qquad N_{\theta g} = N_{\psi g} + (1+\cos\psi) \sum_{m=1}^{4} A_m S_m \tag{40}$$

The bending moments are found with equations (20) using the following wall curvature changes.

$$\chi_{\theta g} = \frac{\cos\psi}{R_o} \sum_{m=1}^{4} A'_m s_m, \qquad \chi_{\psi g} = \chi_{\theta g} + \frac{(1+\cos\psi)}{R_o} \sum_{m=1}^{4} A'_m S_m \tag{41}$$

Again, the preceding functions, constants A_m and A'_m, and computation of series coefficients are discussed further in the appendices.

(b) Particular Solutions - Particular solutions applicable to the nosecap depend on temperature functions (35) and (38) that vary with cos ψ in the examples of Part VIII. These solutions are written below in closed form.

$$N_{\psi p} = N_{\theta p} = A_o \cos \psi, \qquad \chi_{\psi p} = \chi_{\theta p} = -A_o' \cos \psi \tag{42}$$

They are equal in pairs, and A_o and A_o' are constants that are evaluated from temperature data in Part VI and in the appendices.

4. DISPLACEMENTS

(a) Wall Extension - For the nosecap of Figure 2, equation (27) reduces to

$$w = w_o \sin \psi - (1+\nu) R_o Q_\psi / Eh \tag{43}$$

where Q_ψ is defined by integral (8) and computed in Reference [27].

(b) Radial Displacement - The radial component of displacement (u) is obtained from equations (28) and (43) as

$$u = \frac{R_o}{Eh} \left[(N_2 - \nu N_1) + (1 + \nu) N_\psi \right] - w_o \cos \psi \tag{44}$$

where the coordinates are shown in Figure 2, and the other terms are given in the list of nomenclature. The foregoing relations for u and w are also developed in Appendix G.

VIII. NUMERICAL EXAMPLES

1. BICENTRIC-OGIVE RADOME

(a) Thermal Stresses - Based on stress equations presented in the preceding text and the appendices, a computer program was set up for stress analysis of the bicentric-ogive radome described in Reference [23].

The computed stresses were obtained for the temperature distribution given by equations (29) and (30) using the outer-surface straight-line spanwise temperature distribution (T_a) shown in Figure 3 along the mainbody as written below.

$$T_a = 589 + 705 \cos \psi \tag{45}$$

Along the nosecap, the temperatures were represented by

$$T_a = 50 + 1269 \cos \psi \tag{46}$$

which approximates the points plotted near the left side of Figure 3 between z = 28" and 32".

Computerized thermal stresses are listed in Tables 1 and 2 and plotted on Figure 6, which follow immediately.

(b) Displacements - The thermoelastic displacements were computed with equations (27) and (28) for the mainbody and (43) and (44) for the nosecap. The numerical results are tabulated in Table 3 and illustrated in Figure 7.

2. RADOME BASE CONNECTIONS

Four kinds of attachment of a radome base are symbolically illustrated in Figure 8. A stiff connection is indicated by 8a while 8b is flexible. The attachments represented by 8c and 8d are intermediate between the stiff and flexible connections diagrammed in 8a and 8b.

3. THICK-WALLED HEMISPHERICAL RADOME

For purposes of comparison, a thick-walled ($R_o/h = 1.056$) hemispherical radome was analyzed using the temperature functions given by equations (29) to (32), inclusive. Stress values from the computer program are reported in Tables 4 and 5 and plotted on Figure 9. Components of displacement are listed in Table 6 and shown on Figure 10.

4. THIN-WALLED HEMISPHERICAL RADOME

In the third example, stresses were calculated for the thin-walled ($R_o/h = 26.5$) hemispherical radome sketched on Figure 11. For comparison with examples one and two, the same temperature distributions were used. They are defined by equations (29) to (32), inclusive.

The thermal-stress values are presented in Tables 7 and 8 and shown on Figure 11. The computed thermoelastic displacements are listed in Table 9 and plotted on Figure 12.

IX. DISCUSSION

1. NUMERICAL EXAMPLES

(a) First Example - The thermal stresses and displacements that are presented in Tables 1, 2, and 3 for the bicentric-ogive radome are illustrated in Figures 6 and 7. They were computed with $\nu = 0.244$ and $E = 16{,}400{,}000$ psi as mean values for Pyroceram 9606 as described in Appendix A-4 and Reference [19]. Also, the straight-line spanwise temperature distributions given by equations (45) and (46) were employed in the computations. Thickness distributions found in Reference [22] and depicted in Figure 4 are defined by equations (29) and (30).

Table 1. Meridian Stress, σ_ψ, psi (Figure 6)

$\frac{y}{c}$	Coordinate Angle, ψ, Degrees						
	0	30	64°19'23"	68°31'56"	73°44'23"	81°53'25"	90
+1.00	-33,580	-32,910	-23,302	-29,425	-28,615	-25,121	-29,448
+0.75	-16,927	-16,769	-11,601	-18,304	-18,124	-16,123	-19,995
+ .50	- 6,470	- 6,503	- 2,944	- 9,885	- 9,903	- 8,695	-11,398
+ .25	+ 3,699	+ 3,493	+ 5,621	- 1,552	- 1,762	- 1,338	- 2,860
0	+11,459	+11,104	+12,038	+ 4,639	+ 4,245	+ 3,898	+ 3,571
- .25	+16,704	+16,299	+16,944	+ 9,401	+ 8,924	+ 7,971	+ 9,009
- .50	+19,010	+18,634	+19,718	+12,075	+11,570	+10,098	+12,593
- .75	+18,457	+18,239	+20,997	+13,334	+12,900	+11,075	+15,193
-1.00	+15,377	+15,465	+21,306	+13,676	+13,380	+11,305	+17,157

Table 2. Hoop Stress, σ_θ, psi (Figure 6)

$\frac{y}{c}$	Coordinate Angle, ψ, Degrees						
	0	30	64°19'23"	68°31'56"	73°44'23"	81°53'25"	90
+1.00	-33,580	-32,899	-53,818	-30,254	-28,901	-25,445	-31,846
+0.75	-16,927	-16,784	-42,117	-19,022	-18,494	-16,397	-23,715
+ .50	- 6,470	- 6,548	-33,460	-10,905	-10,356	- 8,918	-16,441
+ .35	+ 3,695	+ 3,411	-24,895	- 2,042	- 2,298	- 1,509	- 9,227
0	+11,459	+10,976	-18,479	+ 4,268	+ 3,627	+ 3,779	+ 4,122
- .25	+16,704	+16,113	-13,572	+ 9,153	+ 8,225	+ 7,905	- 11
- .50	+19,010	+18,372	-10,798	+11,953	+10,790	+10,086	+ 2,245
-1.00	+15,377	+14,949	- 9,210	+13,818	+12,441	+11,399	+ 4,149

Table 3. Thermoelastic Displacements (Figure 7)

(Deg-min-sec)	r_c (in)	z_c (in)	(in x 10^3)	(in x 10^3)	(in x 10^3)	(in x 10^3)
0	0	28,175	23.6411	0	0	23.6411
30	0.132	28,060	20.4585	-11.6288	+0.1584	23.5319
64-19-23	0.238	28.025	9.8718	-20.9448	-0.1785	23.1540
66-20-21	1.188	25.957	9.4295	-19.3686	+0.8638	21.5247
68-31-56	2.138	23.671	8.6435	-17.8434	1.5136	19.7688
70-57-49	3.088	21.096	7.8290	-16.2209	2.1101	17.8874
73-44-23	4.038	18.110	6.8369	-14.4297	2.5231	15.7669
75-55-48	4.685	15.724	6.3032	-13.0757	2.9353	14.2158
78-31-17	5.331	12.871	5.5926	-11.5193	3.1884	12.4018
81-53-25	5.978	9.124	4.7401	- 9.5873	3.3403	10.1601
90	6,625	0	0	0	0	0

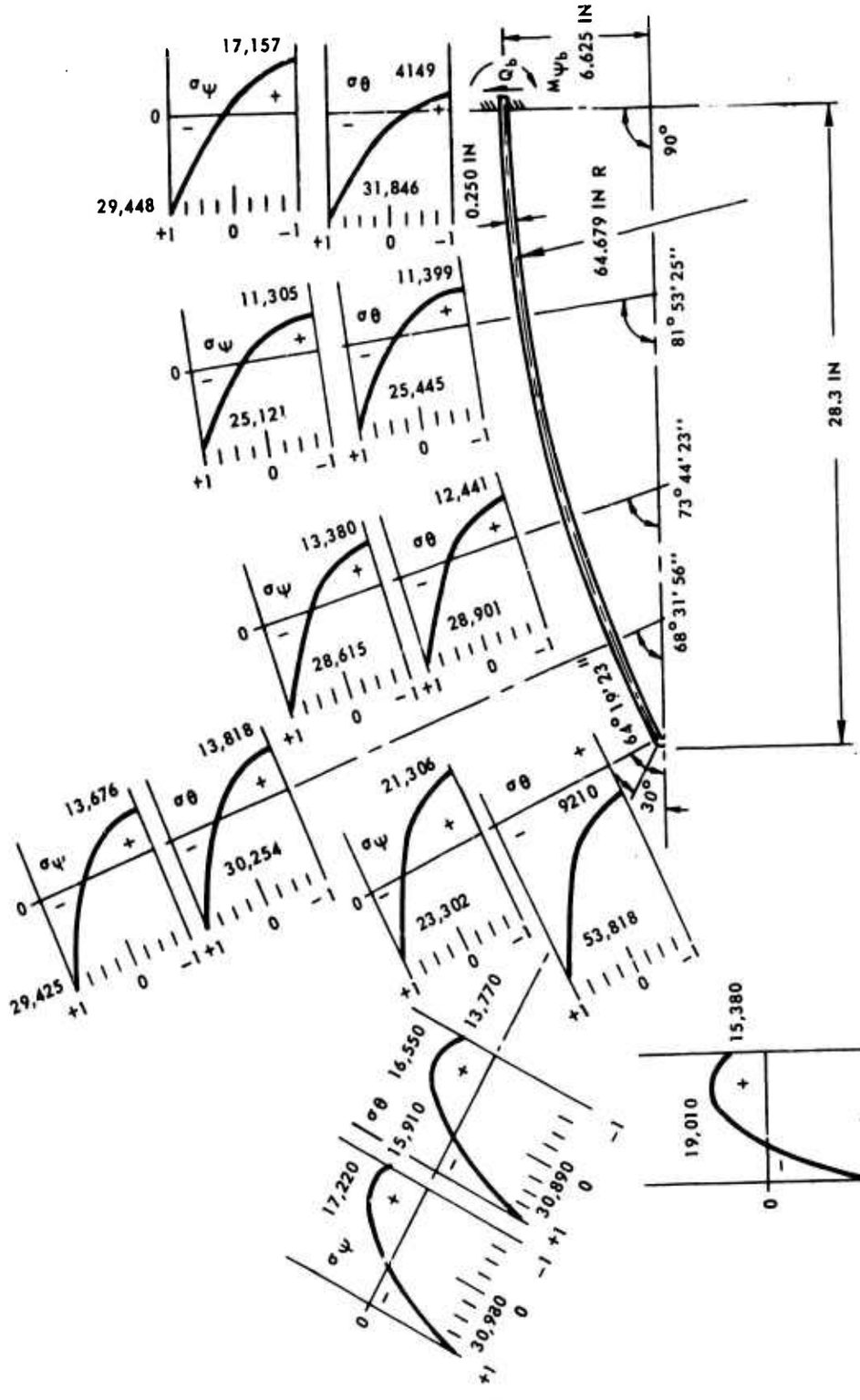

Fig. 6 THERMAL STRESS DISTRIBUTION FOR A BICENTRIC-OGIVE RADOME

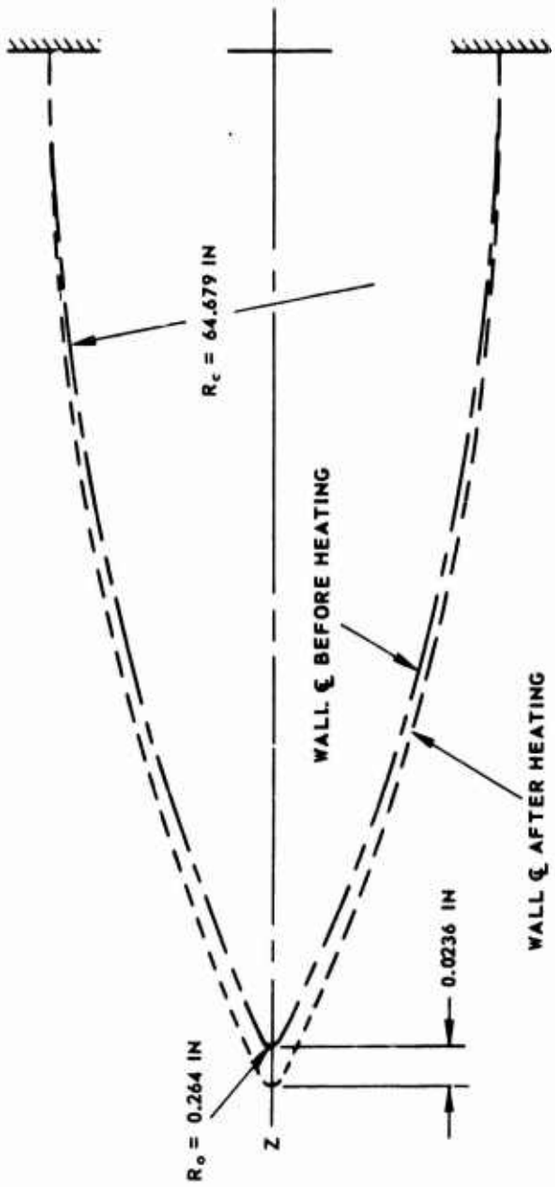

Fig. 7 DISPLACED POSITION OF BICENTRIC-OGIVE RADOME WALL

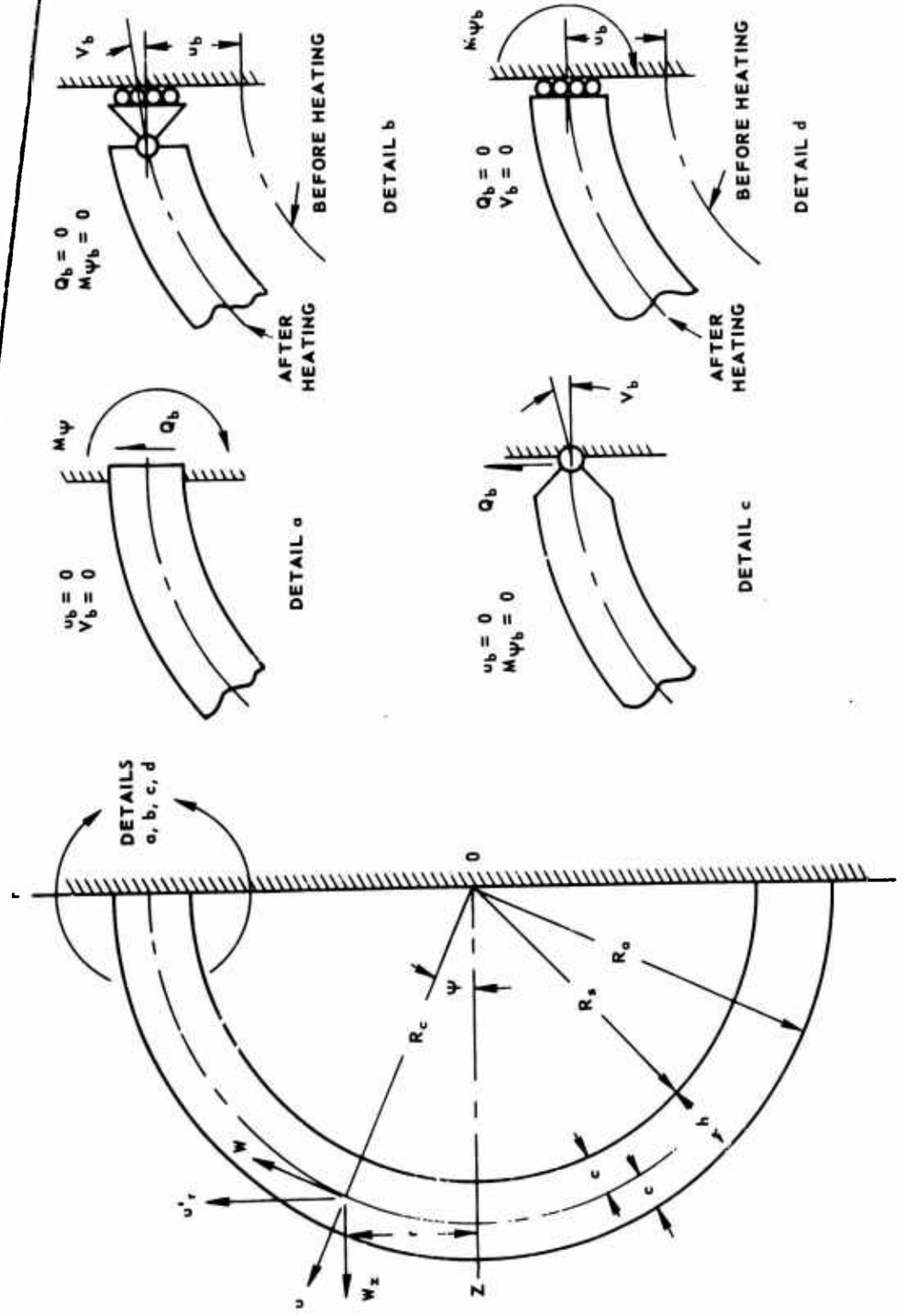

Fig. 8 METHODS OF ATTACHMENT AT BASE OF RADOME

Table 4. Meridian Stress, σ_ϕ, psi (Figure 9).

y/c	Coordinate Angle, ϕ, Degrees						
	0	15	30	45	60	75	90
+1.00	-33,878	-34,194	-35,075	-36,980	-40,348	-45,757	- 53,849
+0.75	-18,333	-18,775	-20,166	-22,687	-26,600	-32,216	- 39,890
+ .50	- 8,954	- 9,369	-10,633	-12,804	-15,958	-20,177	- 25,591
+ .25	- 58	- 406	- 1,421	- 3,017	- 5,053	- 7,349	- 9,776
0	+ 6,165	+ 5,936	+ 5,336	+ 4,619	+ 4,187	+ 4,527	+ 6,068
- .25	+ 9,542	+ 9,540	+ 9,692	+10,452	+12,524	+16,753	+ 23,917
- .50	+ 9,454	+ 9,803	+11,091	+14,026	+19,692	+29,382	+ 44,302
- .75	+ 5,697	+ 6,591	+ 9,632	+15,855	+26,844	+44,479	+ 70,516
-1.00	- 1,983	- 257	+ 5,446	+16,630	+35,588	+65,032	+107,500

Table 5. Hoop Stress, σ_θ, psi (Figure 9).

y/c	Coordinate Angle, ϕ, Degrees						
	0	15	30	45	60	75	90
+1.00	-33,878	-34,248	-35,324	-36,957	-38,732	-39,682	-37,800
+0.75	-18,333	-18,942	-20,705	-23,394	-26,483	-28,893	-28,569
+ .50	- 8,954	- 9,615	-11,516	-14,382	-17,625	-20,133	-19,904
+ .25	- 58	- 749	- 2,723	- 5,650	- 8,882	-11,277	-10,915
0	+ 6,165	+ 5,473	+ 3,516	+ 683	- 2,315	- 4,315	- 3,513
- .25	+ 9,542	+ 8,924	+ 7,216	+ 4,860	+ 2,630	+ 1,679	+ 3,625
- .50	+ 9,454	+ 8,987	+ 7,755	+ 6,267	+ 5,354	+ 6,143	+ 9,982
- .75	+ 5,697	+ 5,503	+ 5,120	+ 5,132	+ 6,432	+10,076	+17,014
-1.00	- 1,983	- 1,741	- 770	+ 1,611	+ 6,369	+14,447	+26,012

Table 6. Thermoelastic Displacements (Figure 10).

ϕ (Deg.)	u (in. x 10^4)	w (in. x 10^4)	u_r (in. x 10^4)	w_z (in. x 10^4)
0	4.798	0	0	4.798
15	4.540	-0.431	0.759	4.496
30	3.806	- .762	1.243	3.677
45	2.722	- .907	1.283	2.566
60	1.502	- .814	0.894	1.456
75	0.457	- .483	0.317	0.585
90	0	0	0	0

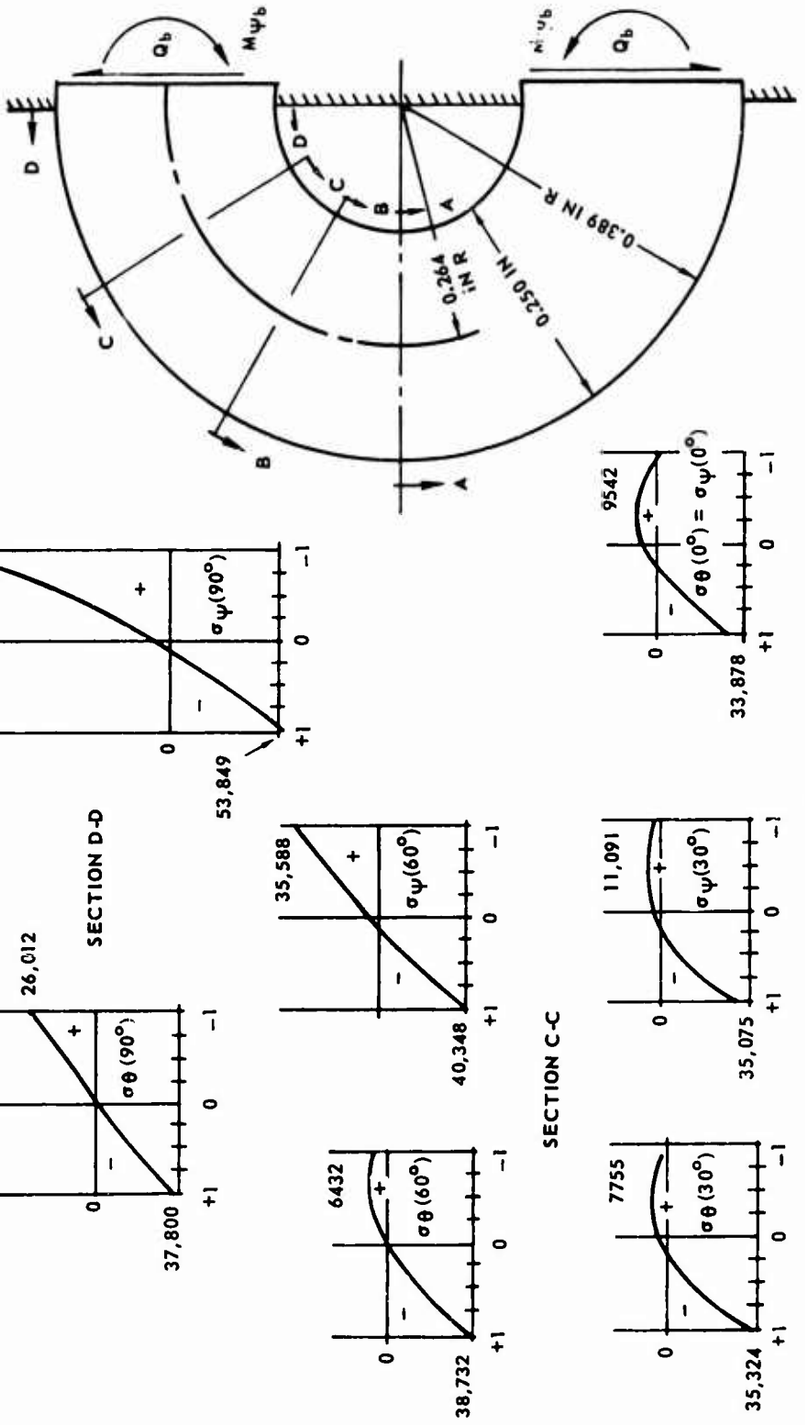

Fig. 9 THERMAL STRESS DISTRIBUTION FOR A THICK-WALLED RADOME

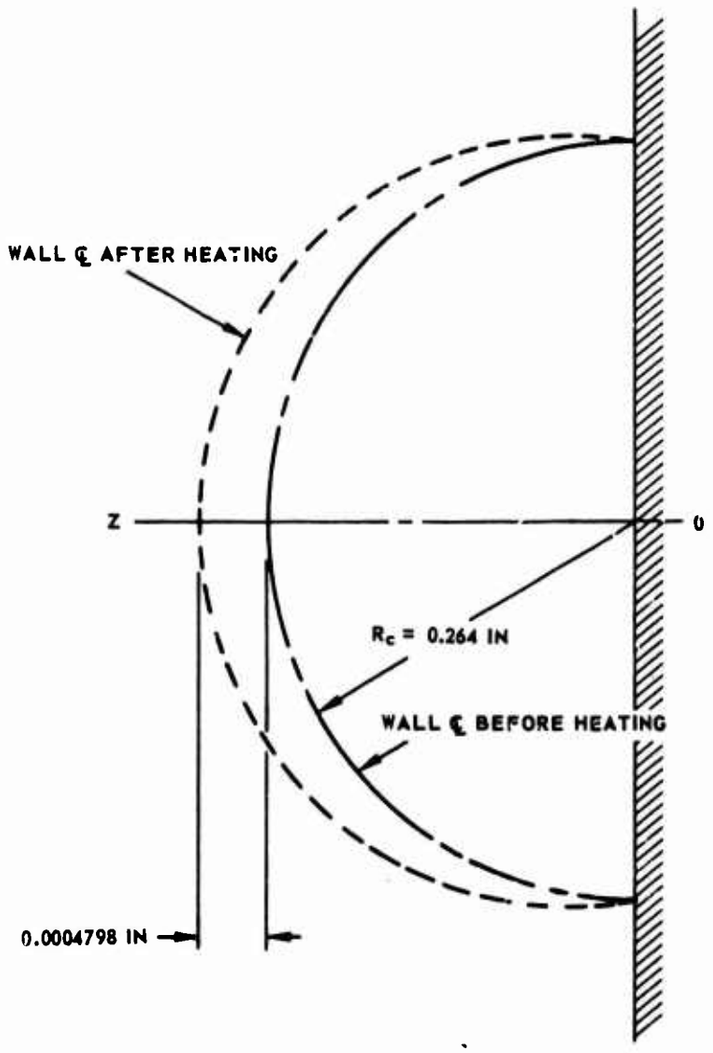

Fig. 10 DISPLACED POSITION OF A THICK RADOME WALL

Table 7. Meridian Stress, σ_ψ, psi (Figure 11).

y/c	Coordinate Angle, ψ, Degrees						
	0	15	30	45	60	75	90
+1.00	-41,856	-41,197	-39,246	-36,281	-32,959	-24,851	-6,219
+0.75	-24,882	-24,538	-23,515	-21,997	-20,422	-15,375	-2,514
+ .50	-13,809	-13,608	-13,011	-12,136	-11,263	- 8,069	+ 295
+ .25	- 2,869	- 2,809	- 2,630	- 2,388	- 2,200	- 848	+3,006
0	+ 5,870	+ 5,793	+ 5,564	+ 5,188	+ 4,711	+ 4,235	+2,569
- .25	+12,426	+12,251	+11,732	+10,928	+10,035	+ 8,009	+3,099
- .50	+16,489	+16,239	+15,494	+14,362	+13,186	+ 9,757	+ 733
- .75	+18,388	+18,103	+17,249	+15,978	+14,765	+10,207	-2,657
-1.00	+18,886	+18,591	+17,705	+16,416	+15,326	+ 9,816	-6,727

Table 8. Hoop Stress, σ_θ psi (Figure 11).

y/c	Coordinate Angle, ψ, Degrees						
	0	15	30	45	60	75	90
+1.00	-41,856	-41,197	-39,270	-36,308	-32,246	-25,066	-28,906
+0.75	-24,882	-24,537	-23,535	-22,035	-19,830	-15,077	-22,190
+ .50	-13,809	-13,607	-13,025	-12,186	-10,792	- 7,253	-16,341
+ .25	- 2,869	- 2,807	- 2,640	- 2,449	- 1,850	+ 491	-10,562
0	+ 5,870	+ 5,795	+ 5,558	+ 5,115	+ 4,938	+ 6,102	- 6,901
- .25	+12,426	+12,254	+11,731	+10,844	+10,137	+10,409	- 4,245
- .50	+16,489	+16,242	+15,498	+14,266	+13,163	+12,694	- 3,454
- .75	+16,489	+16,242	+15,498	+14,266	+13,163	+12,694	- 3,659
-1.00	+18,886	+18,596	+17,719	+16,296	+15,049	+13,845	- 4,511

Table 9. Thermoelastic Displacements (Figure 12).

	u (in. x 10^3)	w (in. x 10^3)	u_r (in. x 10^3)	w_z (in. x 10^3)
0	7.694	0	0	7.694
15	+7.539	-0.107	+1.941	7.285
30	+7.078	- .209	+3.521	6.140
45	+6.314	- .245	+4.447	4.482
60	+5.485	- .278	+4.736	2.767
75	+5.105	-1.714	+4.887	1.487
90	-1.123	0	-1.123	0

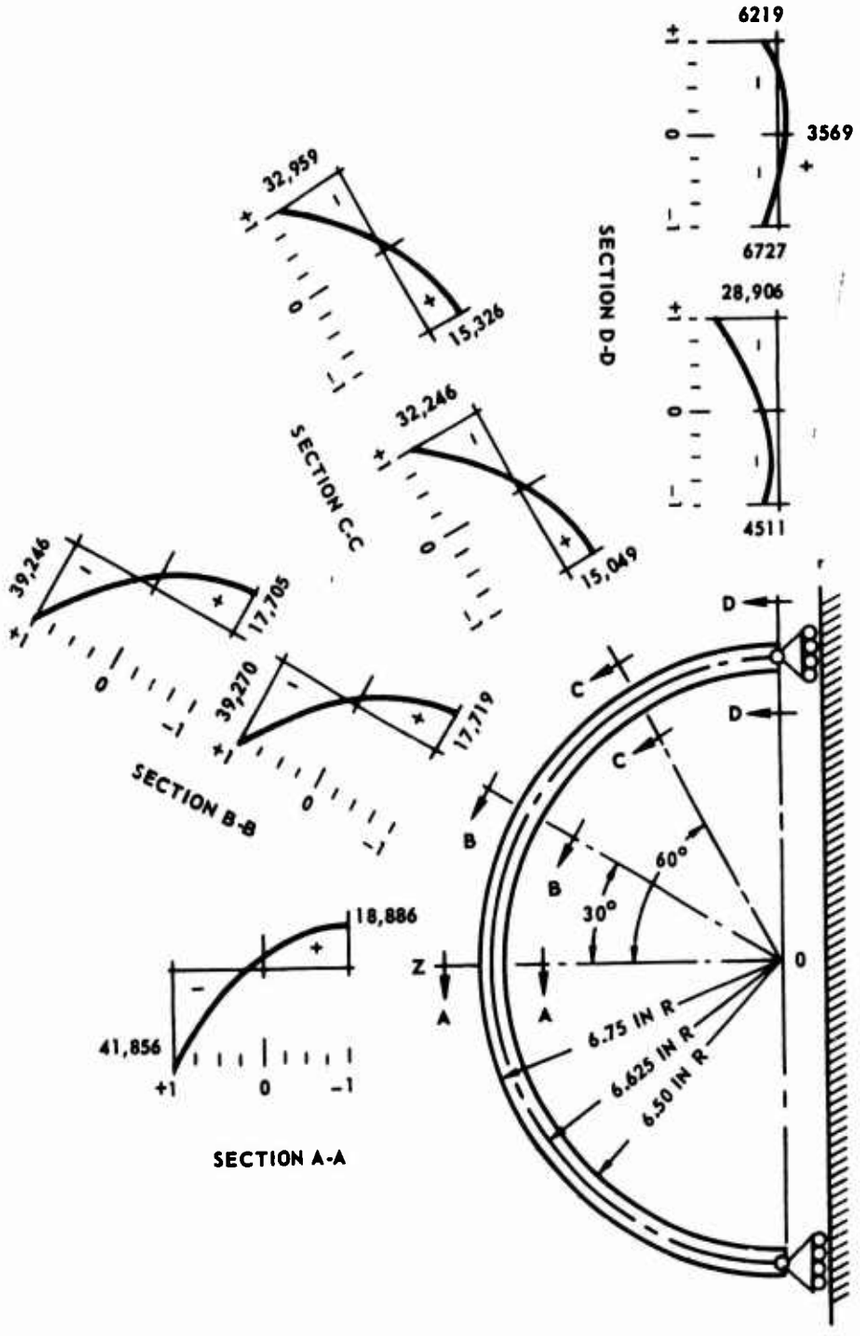

Fig. 11 THERMAL STRESS DISTRIBUTION FOR A THIN-WALLED RADOME

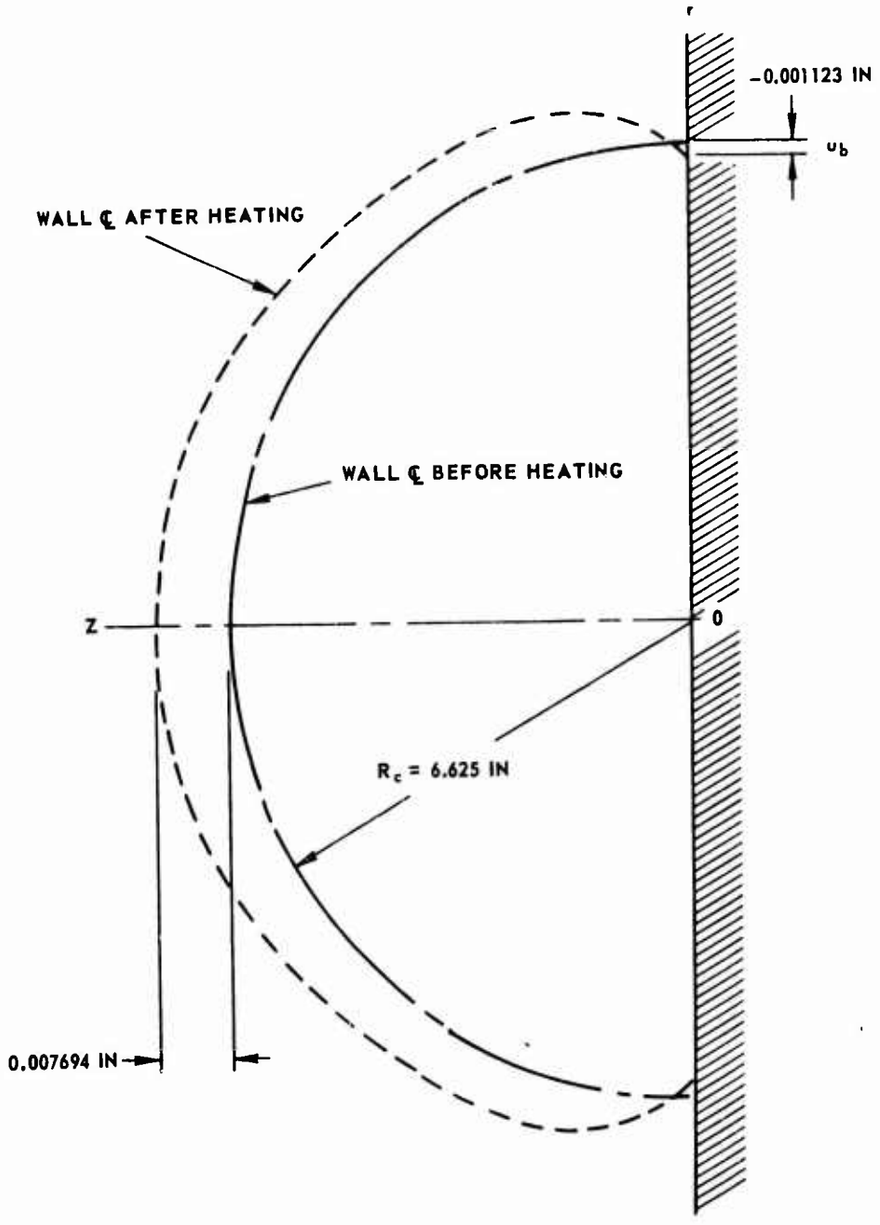

Fig. 12 DISPLACED POSITION OF A THIN RADOME WALL

In all of the tables and figures, negative values denote compressive stresses and positive values are tensile stresses. Component u (Figure 8) of displacement is positive radially outward along the R-axis, and w is positive with increasing ψ. For the rectangular components of displacement, w_z is positive in the positive direction of the Z-axis, and u_r is positive in the direction of increasing r which rotates about the Z-axis as located by the coordinate angle θ.

As shown on Figures 6 and 7 the bicentric-ogive radome is fixed at the base. Various kinds of radome-missile attachments with regard to joint stiffness or flexibility are illustrated in symbolic form on Figure 8.

From the numerical results, it is seen that the stresses generally decrease from the tip to the base of the radome. The maximum tensile hoop stress of 19,010 psi at the tip of the nosecap is less than the allowable material strength of 35,000 psi. In the mainbody, the meridian stress along the inner surface of the wall decreased from +21,310 psi at 64°19'23" to +13,680 psi at 68°31'56". This finding is consistent with the 18,000 psi calculated from measured strains between these two interior points as referred to in Part VI-2b on strength data.

(b) Second Example - For the thick-walled hemispherical radome in this example, the base attachment is shown by Detail "a" of Figure 8, and the dimensions are given in Figures 9 and 10.

From the numerical results in Tables 4 and 5, it is seen that the stresses increase from the tip to the base of the radome while the converse occurred in the previous example. These stresses are excessive and would crack a real radome. Distributions of these thermal stresses are plotted in Figure 9 for comparison only. And the displaced position of the radome wall caused by aerodynamic heating is sketched in Figure 10.

(c) Third Example - The base connection is represented by Detail "b" of Figure 8 for the thin-walled hemispherical radome in this example, and the dimensions are shown in Figures 11 and 12. Also, the radome wall has the same thickness and its central-surface radius is the same as the base radius of the bicentric-ogive radome in the first example.

From the tabulated numerical results (Tables 7 and 8 and Figure 11), one observes that the maximum stresses occur at the tip. There is 18,890 psi tension along the inner surface and 41,860 psi compression along the outer surface of the wall at the tip of the radome. Meridian tensile stress maxima decrease from tip to base along the span and fall inside the wall beyond 45°, while the compressive maxima remain along the wall's outer surface and decrease along the span to 6220 psi at the base.

Again, as shown here in Figure 12, the wall expands outward over most of the length, but is induced by the spanwise heating to move inward at the base. With the stiff base attachments employed in examples one (Figure 7) and two (Figure 10), such inward movement is suppressed.

2. SUMMARY

(a) General Remarks - With fixed ends, examples one and two, displacement and wall-slope change are prevented at the base of a radome; i.e., the boundary conditions imposed by the radome-missile joint are: $V_b = u_b = w_b = 0$, which represent conditions that are more severe than occur in actual structures. A missile body expands and contracts with changing temperatures, so u_b would not vanish.

The bicentric-ogive radome wall material was found to sustain the thermal stresses by both test and theory. Of the two hemispherical radomes that were analyzed for purposes of comparison, the thick-walled radome is overstressed, but stresses in the thin-walled hemisphere lie within safe limits.

(b) Recommendations - It appears that the methods of analysis of thermal stresses and displacements in ogival radomes under aerodynamic heating that are presented herein are satisfactory for numerical evaluations. Further study of the problem is needed, however, to provide answers to unresolved questions.

It is therefore recommended that the investigations be continued to obtain information on nose temperatures, stress maxima, and the effect of different kinds of radome-missile connections.

X. CONCLUSIONS

Based on the reported investigations, it is concluded that:

(1) The methods of analysis are satisfactory for the calculation of thermal stress and displacement in ogival radomes.

(2) Additional information is required on temperature distributions.

(3) Further studies are necessary on nosecap behavior and thermal stress maxima.

(4) Further investigation of radome-missile joint effects is desirable.

APPENDIX A: THEORY

1. EQUILIBRIUM REQUIREMENTS

(a) Stress Equations of Equilibrium - The volume element in Figure 1 is oriented with respect to meridian lines (located from the center of curvature by radius R) and the angle ψ, which measures the inclination of R. The third coordinate is θ, which is the rotational angle about the geometric Z-axis for the ogival body of revolution. They are often referred

to as the natural ogive coordinates. Orthogonal coordinate systems (R, θ, ψ) and (r, θ, z) are shown in Figure 1a.

For axially symmetric bodies and heat distributions, the partial differential equations of equilibrium for a volume element follow immediately.

$$\frac{\partial(rR\sigma_y)}{\partial y} + \frac{\partial(r\tau_{y\psi})}{\partial\psi} = r\sigma_\psi + R\sigma_\theta \sin\psi, \qquad \frac{\partial(rR^2\tau_{y\psi})}{\partial y} + \frac{\partial(rR\sigma_\psi)}{\partial\psi} = R^2\sigma_r \cos\psi \tag{47}$$

Equations (47) are derived from $\Sigma F_y = 0$ and $\Sigma F_\psi = 0$, respectively. Owing to geometrical and thermal symmetry, there are no changes in the θ direction and $\tau_{y\theta}$ and $\tau_{\psi\theta}$ are zero as well as $\Sigma F_\theta = 0$.

(b) Stress and Moment Resultants - When equations (47) are integrated over the wall thickness, the equations of equilibrium are obtained in terms of the stress and moment resultants of integrals (6), (8), and (10).

$$\frac{d(r_c Q_\psi)}{d\psi} = (r_c N_\psi + R_c N_\theta \sin\psi) - (r_a R_a p_{ay} + r_s R_s p_{sy}) \tag{48}$$

$$\frac{d(r_c N_\psi)}{d\psi} = (R_c N_\theta \cos\psi - r_c Q_\psi) - (r_a R_a p_{a\psi} + r_s R_s p_{s\psi}) \tag{49}$$

$$\frac{d(r_c M_\psi)}{d\psi} = R_c(M_\theta \cos\psi + r_c Q_\psi) + c(r_s R_s p_{s\psi} - r_a R_a p_{a\psi}) \tag{50}$$

In the foregoing relations, p_{ay} and $p_{a\psi}$ are the radial and tangential components of pressure at the outer surface of the radome; and p_{sy} and $p_{s\psi}$, at the inner surface. These pressures are equated to zero in a thermal-stress problem.

For the investigation of temperature stresses, therefore, the resultant stress and moment conditions that ensure equilibrium are expressed as follows.

$$N_\psi = Q_\psi \cot\psi, \qquad N_\theta = \frac{d(r_c Q_\psi / R_c \sin\psi)}{d\psi}, \qquad \frac{d(r_c M_\psi)}{R_c d\psi} = M_\theta \cos\psi + r_c Q_\psi \tag{51}$$

These expressions hold for both thick and thin-walled ogive shells from the inner apex to attachment points at the missile body, but not within the attachment region owing to restraints set up by the connections. In any case,

however, the body-joint problem requires further analysis and can often be treated by reintroducing the surface pressures as derived in equations (48) to (50), inclusive.

2. STRAIN EXPRESSIONS

(a) Thermal Strain - For Pyroceram 9606, the thermal-strain function (ϵ_t) was developed from test data in Reference [19]. From these results together with temperature distributions reported in Reference [22] for wind tunnel testing of a Von Karman radome, the function is defined as follows.

$$\epsilon_t = (-241.2 + 3.445T) \times 10^{-6}, \quad 70° \leq T \leq 400°F \tag{52}$$

$$= (-119.1 + 2.958T) \times 10^{-6}, \quad 200° \leq T \leq 600°F \tag{53}$$

$$= (+190.3 + 2.221T) \times 10^{-6}, \quad 300° \leq T \leq 1400°F \tag{54}$$

Temperature (T) is given by equations (29) to (31), inclusive.

Inspection of the distribution of temperature defined throughout the radome by these equations and Figure 3 revealed that equation (52) satisfactorily describes the temperature in the inside half of the wall ($-1 \leq x \leq 0$) along the entire span; equation (53) defines T over the full span in the quarter thickness above the wall centerline ($0 \leq x \leq +0.5$); and (54) serves the same purpose in the outer quarter of the wall thickness ($+0.5 \leq x \leq +1$). This arrangement expedites the calculation of temperature functions, integrals (7) and (11), and the stress equation (2).

The strains computed with equation (52) agree with the measured data, Reference [19], within -1 to +3 percent. Those calculated from equation (53) correspond to the measurements within five percent; and the ones found with (54) agree within seven percent in the low part of the temperature range, which is seldom used, and deviations in the upper half of the range lie between approximately -2 and +4 percent.

(b) Actual Strain - Components of strain for elastic behavior were thoroughly discussed by Love [1] and other authors [2], [3], [4], and [5]. We have

$$\epsilon_\psi = (\epsilon_{\psi c} - y\chi_\psi)R_c/R, \qquad \epsilon_\theta = (\epsilon_{\theta c} - y\chi_\theta)r_c/r \tag{55}$$

$$\epsilon_{\psi c} = \frac{1}{R_c}\left[u + \frac{dw}{d\psi}\right], \qquad \epsilon_{\theta c} = \frac{1}{r_c}\left(u \sin\psi + w \cos\psi\right) \tag{56}$$

$$V = \frac{1}{R_c}\left[\frac{du}{d\psi} - w\right], \qquad \chi_\psi = \frac{1}{R_c}\frac{dV}{d\psi}, \qquad \chi_\theta = \frac{V\cos\psi}{r_c} \tag{57}$$

where equations (55) define the normal-strain components at any point in the wall of the radome, equations (56) give these strains at the central surface, and (57) shows the change (V) of the slope of the wall together with curvature changes. General solutions for the latter functions appear as equations (22); and particular solutions, as equations (25) and (26).

(c) Elastic Strain - As the result of thermal strain due to temperature change plus elastic strain produced by constraints against thermal expansion or contraction, we have

$$e_\psi = \epsilon_\psi - \epsilon_t, \qquad e_\theta = \epsilon_\theta - \epsilon_t \tag{58}$$

where e_ψ, e_θ are the components of elastic strain in the wall of the heated radome. And the other terms are given by equations (55) to (57), inclusive.

3. MECHANICAL PROPERTIES

(a) Young's Modulus - Dependence on temperature of the mechanical properties of Pyroceram 9606 was examined in Reference [19]. In the present numerical examples, an average value of E was employed and is written below.

$$E = E_{av} = 16{,}400{,}000 \text{ psi}; \qquad 70^\circ \le T \le 1400^\circ F \tag{59}$$

Values of E over the above temperature range, which includes all temperatures in the examples, agree within four percent of the quoted average.

(b) Poisson's Ratio - As pointed out in Reference [19], Poisson's ratio (ν) is nearly constant for the radome-wall material. For the specified temperature range, its mean value is

$$\nu = \nu_{av} = 0.244, \qquad 70^\circ \le T \le 1400^\circ F \tag{60}$$

and the largest differences between this mean value and the test data amount to ±2.5 percent.

4. STRESS STRAIN RELATIONS

(a) Hooke's Law - The previously discussed wall stresses and strains are related by means of Hooke's law; e.g.,

$$Ee_\psi = \sigma_\psi - \nu\sigma_\theta, \qquad Ee_\theta = \sigma_\theta - \nu\sigma_\psi \tag{61}$$

from which the stresses are customarily expressed in the following manner.

$$\sigma_\psi = E'(e_\psi + \nu e_\theta), \quad \sigma_\theta = E'(\nu e_\psi + e_\theta), \quad E' = E/(1 - \nu^2) \tag{62}$$

As presented in the next two articles, the preceding relationships let us express the central-surface strains and curvature changes in terms of the stress and moment resultants.

(b) Normal-Stress Resultants - When E and ν are represented by their constant mean values, equations (59) and (60) respectively, the integrals (5), (6), and (7) together with equations (55) to (58) and (62) lead to the following expressions for N_1 and N_2.

$$N_1 = E'h(\epsilon_{\psi c} + \nu\epsilon_{\theta c}), \qquad N_2 = E'h(\nu\epsilon_{\psi c} + \epsilon_{\theta c}) \tag{63}$$

Second and higher order effects are neglected in this calculation of N_1 and N_2 in terms of the central-surface strain components.

(c) Bending Moments - Equations (9), (10), and (11) are used with (55) to (61), inclusive, to obtain

$$M_1 = -D(\chi_\psi + \nu\chi_\theta), \qquad M_2 = -D(\nu\chi_\psi + \chi_\theta) \tag{64}$$

wherein the second-order effects are again neglected, D is the wall flexural stiffness factor stated by equation (21), and the curvature-change components are given by equations (22) and (57).

APPENDIX B: TEMPERATURE FUNCTIONS

1. NORMAL-STRESS TEMPERATURE FUNCTIONS

Functions that depend on the temperature distribution and have the dimensions of a normal-stress resultant are defined by equations (7) and can be expressed in the forms written below.

$$N_{t\theta} = K_0 + K_1 \cos\psi, \qquad N_{t\psi} = N_{t\theta} + (K_2 + K_3 \cos\psi)R_c/r_c \tag{65}$$

When equations (2), (29), (30), (31), (52), (53), (54), (59), and (60) are substituted into (7) and integrated, the K_i are found to have the following values.

$$K_0 = 4.648Eh/(1-\nu) \times 10^4, \qquad K_1 = 6.792Eh/(1-\nu) \times 10^4 \tag{66}$$

$$K_2 = 4.393Eh/(1-\nu) \times 10^7, \qquad K_3 = 3.420Eh/(1-\nu) \times 10^7 \tag{67}$$

The radii r_c and R_c that occur in equation (65) are illustrated in Figure 1 and defined by equations shown on the figure. They are evaluated in Reference [25].

2. BENDING-MOMENT TEMPERATURE FUNCTIONS

Functions that depend on the temperature distribution and have the dimensions of a bending-moment resultant are defined by equations (11) and can be expressed in the forms written below.

$$M_{t\theta} = J_0 + J_1 \cos\psi, \qquad M_{t\psi} = M_{t\theta} + (J_2 + J_3 \cos\psi)R_c/r_c \tag{68}$$

When equations (2), (29), (30), (31), (52), (53), (54), (59), and (60) are substituted into (11) and integrated, the J_i are found to have the following values.

$$J_0 = 1.269Eh^2/(1-\nu) \times 10^4, \qquad J_1 = 0.989Eh^2/(1-\nu) \times 10^4 \tag{69}$$

$$J_2 = 1.704Eh^2/(1-\nu) \times 10^7, \qquad J_3 = 2.195Eh^2/(1-\nu) \times 10^7 \tag{70}$$

One can see that the K_i have the dimensions of pounds per inch (ppi); and the J_i, of inch-pounds per inch (ippi). Again the above are evaluated in Reference [25].

APPENDIX C: DIFFERENTIAL EQUATIONS FOR SHEAR AND SLOPE FUNCTIONS

1. AUXILIARY SHEAR FUNCTION

To find solutions for the total shear (Q_ψ), equation (8), the auxiliary shear function (q) is introduced such that

$$q = r_c Q_\psi / R_c \sin\psi, \qquad N_\psi = \frac{R_c q \cos\psi}{r_c}, \qquad N_\theta = \frac{dq}{d\psi} \tag{71}$$

and, by solving equations (63), the central-surface normal strains are obtained in terms of q.

From equations (56) and (57), V is found in terms of the central-surface normal strains.

$$V = \frac{\csc\psi}{R_c} \frac{d(r_c \epsilon_{\theta c})}{d\psi} - \epsilon_{\psi c} \cot\psi \tag{72}$$

And with equations (5), (63), and (71) put into (72), the following ordinary differential equation is obtained

$$(L^2 + \nu)q = EhV + (N_{t\psi} - \nu N_{t\theta})\cot\psi - \frac{\csc\psi}{R_c} \frac{d}{d\psi}\left[r_c (N_{t\theta} - \nu N_{t\psi}) \right] \tag{73}$$

The operator L^2 is defined as follows:

$$L^2 q = \frac{r_c \csc\psi}{R_c} \frac{d^2 q}{d\psi^2} + \cot\psi \frac{dq}{d\psi} - \frac{q R_c \cos\psi}{r_c \tan\psi} \tag{74}$$

and, in general, the solutions of equation (73) are obtained as infinite series for q and V, which are exemplified by equations (12) and obtained in Reference [26].

2. WALL-SLOPE CHANGE

Relationships similar to the foregoing are derived for V by substitution of equations (11), (22), and (23) into (51). The result is

$$(L^2 - \nu)(EhV) = (\beta^4 + \nu^2)\left[\frac{M_{t\theta} \cot\psi}{R_c} - q - \frac{\csc\psi}{R_c^2} \frac{d(r_c M_{t\psi})}{d\psi} \right] \tag{75}$$

where L^2 is given by equation (74), q by (71), and the temperature moments by (11) and (68). The wall-bending parameter (β) is calculated with

$$\beta^4 = -\nu^2 + 12(1-\nu^2)(R_c/h)^2 \tag{76}$$

which is developed from the expression EhR_c^2/D, where D is given by equation (21). The general solutions of equation (75) are given in Reference [26].

3. SPECIFIC RESULTS

When specific temperature functions defined by equations (65) and (68) are put into equations (73) and (75), the results are as follows.

$$(L^2+\nu)(q+K_3) = EhV + (1-\nu)K_1 r_c/R_c + K_2 R_c/r_c \tan\psi \tag{77}$$

$$(L^2-\nu)(EhV) = (\beta^4+\nu^2)(J_1 r_c/R_c^2 + J_3/R_c - q) \tag{78}$$

Particular solutions of (77) and (78) are necessitated by the presence of constants K_i, J_i and general solutions when these constants are absent. These solutions are developed in Reference [24].

APPENDIX D: SOLUTION OF EQUATIONS

1. MAINBODY

(a) General Solutions - To find the general solutions of equations (77) and (78), one observes that

$$(L^4+\beta^4)q_g = 0, \qquad (L^4+\beta^4)V_g = 0 \tag{79}$$

where subscript "g" denotes that the solutions are general. They are found as

$$q_g = \frac{r_c}{R_c}\sum_{m=1}^{4} B_m f_m(\psi), \qquad V_g = \frac{r_c}{R_c}\sum_{m=1}^{4} B_m' f_m(\psi) \tag{80}$$

where series f_m (m = 1, 2, 3, 4) are given by equations (12) and (16).

The series coefficients (a_{mn}) are computed from recurrence formulas as explained in Reference [26], and constants B_m and B_m' are related as follows.

$$B_1 = (\nu B_1 + \beta^2 B_2)/Eh, \qquad B_2' = (\nu B_2 - \beta^2 B_1)/Eh \tag{81}$$

And similar relations hold for m = 3 and 4.

(b) Particular Solutions - With reference to equations (77) and (78), only the terms involving r_c as the only variable can be solved in closed form. These forms are asssociated with K_1 and J_1. We have

$$(L^2 + \nu)q_p = EhV_p + (1-\nu)K_1 r_c/R_c \tag{82}$$

$$(L^2 - \nu)(EhV_p) = (\beta^4 + \nu^2)(J_1 r_c/R_c^2 - q_p) \tag{83}$$

and the particular solutions are written below.

$$q_p = B_8 r_c/R_c, \qquad V_p = -B_8' r_c/R_c \tag{84}$$

$$B_8 = \frac{J_1}{R_c} - \frac{(1-\nu^2)(J_1 + R_c K_1)}{(1+\beta^4)R_c}, \qquad B_8' = \frac{(1-\nu)(\nu^2+\beta^4)(J_1 + R_c K_1)}{(1+\beta^4)R_c Eh} \tag{85}$$

These solutions, equations (84), are included in equations (23) and (25). For other terms (the ones that involve K_2, K_3, and J_3), however, infinite expansions are required to satisfy the differential equations. In the current examples, approximation functions are used that meet the requirements with errors of one-half percent or less. The approximate solutions are discussed in Reference [24].

APPENDIX JUNDARY CONDITIONS

1. GENERAL REQUIREMENTS

In general, one considers the requirements at the juncture of two arbitrary segments of the mainbody, such as MB1 and MB2 with the junction at $\psi_3 = 73°44'23"$ in the first numerical example. Eight functions are involved: displacements u, w and slope change V; stress resultants Q_ψ, N_ψ, N_θ; and moments M_ψ, M_θ. At any juncture (ψ_i) where there is wall material and geometric continuity, all eight functional requirements can be met by the following five equations.

$$w(\psi_i+) = w(\psi_i-1), \qquad V(\psi_i+) = V(\psi_i-) \tag{86}$$

$$q(\psi_i+) = q(\psi_i-1), \qquad N_\theta(\psi_i+) = N_\theta(\psi_i-) \tag{87}$$

$$\chi_\psi(\psi_i+) = \chi_\psi(\psi_i-) \tag{88}$$

From these, one constant w_i in $w(\psi_i+)$ is determined directly and four relations for constants of integration B_m are obtained. The equations and evaluation of the constants are discussed in Reference [26].

2. RADOME BASE

At the base of a radome, three equations are found according to the type of attachment as illustrated in Figure 8. In all cases, axial relative displacement between missile and radome vanishes, or

$$w(90^\circ) = w_b = 0 \tag{89}$$

and the constant w_i in w_b is computed directly. Then for a fixed base, we have

$$u(90^\circ) = u_b = 0, \qquad V(90^\circ) = V_b = 0 \tag{90}$$

and for a free base, the requirements are stated below.

$$q(90^\circ) = q_b = 0, \qquad M_\psi(90^\circ) = M_{\psi b} = 0 \tag{91}$$

With a hinged base, one uses

$$u_b = 0, \qquad M_{\psi b} = 0 \tag{92}$$

and with a bearing-supported base

$$q_b = 0, \qquad V_b = 0 \tag{93}$$

where the relationship between q and Q_ψ is given in equation (71).

3. NOSECAP-MAINBODY JUNCTION

At $\psi_1 = 64°19'23''$, which locates the interface between the nosecap and MB1 (Figure 2) in the bicentric-ogive radome of the first example, the requirements for strain continuity lead to the following expressions.

$$\epsilon_{\psi c}(\psi_1 +) = \epsilon_{\psi c}(\psi_1 -), \qquad \epsilon_{\theta c}(\psi_1 +) = \epsilon_{\theta c}(\psi_1 -) \tag{94}$$

$$\chi_\theta(\psi_1 +) = \chi_\theta(\psi_1 -), \qquad R_o\chi_\psi(\psi_1 +) = R_c\chi_\psi(\psi_1 -) \tag{95}$$

$$\epsilon_{\psi c}(\psi_1 -) + R_c\chi_\psi(\psi_1 -) = 0, \qquad \epsilon_{\theta c}(\psi_1 -) + R_o\chi_\theta(\psi_1 -) = 0 \tag{96}$$

Equations (94) and (96) produce satisfaction of

$$Q_\psi(\psi_1 +) = Q_\psi(\psi_1 -), \qquad N_2(\psi_1 +) = N_2(\psi_1 -) \tag{97}$$

which also meet similar requirements imposed on N_ψ and u, since the constant w_o in the nosecap formula for w is computed with the next equation.

$$w(\psi_1 +) = w(\psi_1 -) \tag{98}$$

The first of equations (95) satisfies the requirement on V, equation (86), and the second one fulfills a requirement that is similar to equation (88).

APPENDIX F: THERMOELASTIC DISPLACEMENTS

1. WALL EXTENSION

From equations (56) for the mainbody, we have

$$\epsilon_{\psi c} - \frac{r_c \epsilon_{\theta c}}{R_c \sin\psi} = \frac{\sin\psi}{R_c}\frac{d(w\csc\psi)}{d\psi} = \frac{N_1 - \nu N_2}{Eh} + \frac{r_c(\nu N_1 - N_2)}{R_c Eh \sin\psi}$$

$$= \frac{N_{t\psi} - \nu N_{t\theta}}{Eh} + \frac{r_c(\nu N_{t\psi} - N_{t\theta})}{R_c Eh \sin\psi}$$

$$+ (R_c \sin\psi + \nu r_c)\frac{q\cot\psi}{r_c Eh} - \frac{(r_c + \nu R_c \sin\psi)}{R_c Eh \sin\psi}\frac{dq}{d\psi} \qquad (99)$$

which is integrated to secure equation (27). The integration constant in equation (27) is w_i, and functions w_q and w_t are shown below.

$$w_q = W\sin\psi - \frac{(r_c + \nu R_c \sin\psi)q}{Eh\sin\psi} \qquad (100)$$

$$w_t = \frac{\sin\psi}{Eh}\int\left[(N_{t\theta} - \nu N_{t\psi})r_c \csc\psi + (\nu N_{t\theta} - N_{t\psi})R_c\right]\frac{d\psi}{\sin\psi} \qquad (101)$$

$$W = \frac{H}{Eh}\int\frac{q(2r_c + R_c\sin\psi)\cos\psi\, d\psi}{r_c \sin^3\psi} \qquad (102)$$

When the normal-stress temperature functions in equation (101) are given by equations (65), w_t becomes

$$w_t = \frac{(1-\nu)H}{Eh}(K_0\cos\psi + K_1) + \frac{\nu R_c}{Eh}(K_2\cos\psi + K_3)$$

$$+ \frac{R_c\sin\psi}{Eh\sin\psi_c}\left[K_2(\Lambda_1 + \Lambda_2\sec\psi_c) + K_3\Lambda_3\right] \qquad (103)$$

$$\Lambda_1 = \ell n(\csc\psi - \cot\psi),\ \Lambda_2 = \ell n\left[\frac{1 + \cos(\psi+\psi_c)}{r_c/R_c}\right],\ \Lambda_3 = \ell n(R_c/r_c\csc\psi) \qquad (104)$$

where the Λ_1 are logarithmic expressions as indicated above. The trigonometric sine of the central-surface apex is computed with

$$\sin\psi_c = H/R_c, \qquad H = R_c - r_{bc} \qquad (105)$$

and sec ψ_c can then be readily obtained. Values of the K_i are calculated from equations (66) and (67). Functions W, integral (102), can be computed with infinite series, but it is usually more convenient to find W by finite summation.

2. RADIAL DISPLACEMENT

To find u for the mainbody, we again use the second of equations (56) together with equation (27) for w. When $\epsilon_{\theta c}$ is obtained from equation (63), the following result is found.

$$u = (N_2 - \nu N_1) r_c / Eh \sin \psi - w \cot \psi \tag{106}$$

Equation (106) can be used throughout the ogival mainbody since $\psi > 0$.

APPENDIX G: NOSECAP EXPRESSIONS

1. TEMPERATURE FUNCTIONS

(a) Normal-Stress Temperature Functions - When one uses outer-surface temperature distributions that vary with cos ψ in the manner of equations (45) and (46) for the nosecap, the normal-stress-resultant temperature function, equation (35), can be expressed as follows.

$$N_t = N_{t\psi} = N_{t\theta} = K_0' + K_1' \cos \psi \tag{107}$$

For the nosecap on the bicentric-ogive radome, surface temperatures were given by equation (46), and

$$K_0' = -0.0612Eh/(1-\nu) \times 10^{-4}, \quad K_1' = 13.873Eh/(1-\nu) \times 10^{-4} \tag{108}$$

which were employed in the first example.

For the hemispherical radomes, the surface temperatures were given by equation (45), and

$$K_0' = 5.842Eh/(1-\nu) \times 10^{-4}, \quad K_1' = 7.772Eh/(1-\nu) \times 10^{-4} \tag{109}$$

which were used in the second and third examples.

(b) Bending-Moment Temperature Functions - Since temperature functions for the bending-moment resultant have the same general form as equation (107), one can use

$$M_t = M_{t\psi} = M_{t\theta} = J_o' + J_1' \cos \psi \tag{110}$$

and, for the nosecap with surface temperatures from equation (46), the constants are written below.

$$J_o' = 0.5195Eh^2/(1-\nu) \times 10^{-4}, \quad J_1' = 2.830Eh^2/(1-\nu) \times 10^{-4} \tag{111}$$

For the hemispherical radomes, the surface temperatures were given by equation (45), and

$$J_o' = 1.732Eh^2/(1-\nu) \times 10^{-4}, \quad J_1' = 1.585Eh^2/(1-\nu) \times 10^{-4} \tag{112}$$

which were employed in the second and third numerical examples.

2. DIFFERENTIAL EQUATIONS FOR SHEAR AND SLOPE FUNCTIONS

(a) Total Shear - For hemispherical segments, such as the nosecap, equation (73) reduces to

$$(L^2 + \nu)Q_\psi = EhV - (1-\nu)\frac{dN_t}{d\psi} \tag{113}$$

and equation (74) becomes

$$L^2 Q = \frac{d^2Q}{d\psi^2} + \cot \psi \frac{dQ}{d\psi} - Q \cot^2 \psi \tag{114}$$

which lead to general solutions of the kind indicated by equations (39) and (40) that are more fully described in Reference [27].

(b) Wall-Slope Change - For the nosecap, equation (75) reduces to

$$(L^2 - \nu)(Ehv) = -(\beta_o^4 + \nu^2)\left[Q_\psi + \frac{1}{R_o}\frac{dM_t}{d\psi}\right] \tag{115}$$

where L^2 is given by equation (114), Q_ψ by (8) and the temperature moment by (38) and (110). The general solutions are discussed in Reference [27].

(c) Specific Results - When the specific temperature functions defined by equations (107) and (110) are put into equations (113) and (115), the results are as follows.

$$(L^2+\nu)\,Q_\psi = EhV + (1-\nu)K_1' \sin\psi \tag{116}$$

$$(L^2-\nu)(EhV) = (\beta_o^4+\nu^2)\left[\frac{J_1'\sin\psi}{R_o} - Q_\psi\right] \tag{117}$$

Particular solutions of these equations are necessitated by the presence of constants K_1' and J_1' and general solutions when these constants are absent.

3. SOLUTION OF EQUATIONS

(a) General Solutions - To find general solutions of equations (116) and (117), one observes that

$$(L^4+\beta_o^4)\,Q_g = 0, \qquad (L^4+\beta_o^4)\,V_g = 0 \tag{118}$$

where subscript "g" denotes that the solutions are general. They are found to be

$$Q_g = \sin\psi \sum_{m=1}^{4} A_m a_m, \qquad V_g = \sin\psi \sum_{m=1}^{4} A_m' a_m \tag{119}$$

where the infinite series (s_m) are indicated by the first of equations (39), and they are developed in Reference [27].

(b) Particular Solutions - The terms associated with sin ψ in equations (116) and (117) possess closed-form solutions. They are

$$Q_p = A_o \sin\psi, \qquad V_p = -A_o' \sin\psi \tag{120}$$

where constants A_o, A_o' depend on K_1', J_1' as shown below.

$$A_o = \frac{J_1'}{R_o} - \frac{(1-\nu^2)(J_1'+R_oK_1')}{(1+\beta_o^4)R_o}, \qquad A_o' = \frac{(1-\nu)(\nu^2+\beta_o^4)(J_1'+R_oK_1')}{(1+\beta_o^4)R_o\,Eh} \tag{121}$$

Numerical values of the foregoing constants were obtained with the aid of equations (108), (109), (111), and (112) and used in the three example problems.

4. BOUNDARY CONDITIONS

(a) Nosecap Requirements - The nosecap boundary conditions at its juncture with the mainbody are discussed in Appendix E-3 in conjunction with equations (94) to (98), inclusive. However, owing to errors in the original computer program not all of these conditions were met in the first numerical example. The numerical results reported herein satisfy requirements that meridian fiber stresses at the inner and outer surfaces of the wall are equal between mainbody and nosecap, but there are discontinuities in some of the terms that appear in equations (94) to (97), inclusive. Equation (98) was exactly fulfilled however.

In consequence, the nosecap stresses must be regarded as approximate rather than precise results. Furthermore, they are believed to be reasonably good approximations.

(b) Base Connection Requirements - The base-connection boundary conditions given by equations (89) to (93) were used in comparison studies with hemispherical radomes. They were completely satisfied in these studies. In the second example in this report, conditions (90) were imposed; and in the third example, conditions (91).

5. DISPLACEMENTS

(a) Extension - Extension (w) of the nosecap wall, which is illustrated in Figure 8, is computed from equation (56) with $r_c = R_o \sin\psi$; i.e.,

$$\epsilon_{\psi c} - \epsilon_{\theta c} = \frac{\sin\psi}{R_o}\frac{d(w\csc\psi)}{d\psi} = \frac{(1+\nu)}{Eh}(N_1 - N_2)$$

$$= -\frac{(1+\nu)}{Eh}\sin\psi\frac{d(Q\csc\psi)}{d\psi} \qquad (122)$$

from which the following expression is obtained.

$$w = w_o \sin\psi - (1+\nu)R_o Q/Eh \qquad (123)$$

And w_o is an arbitrary constant.

(b) Radial Displacement - Again using the central-surface hoop strain and equations (56) and (63), one has

$$\epsilon_{\theta c} = (u + w\cot\psi)/R_o = (N_2 - \nu N_1)/Eh \qquad (124)$$

which is solved to obtain the following expression for u.

$$u = (N_2 - \nu N_1)R_o/Eh - w \cot \psi \tag{125}$$

Since cot ψ becomes infinite at $\psi = 0$, it is desirable to substitute equation (123) into (125) for numerical work. In this way, we arrive at the next relationship for the radial displacement (u).

$$u = \frac{R_o}{Eh}\left[(N_2 - \nu N_1) + (1 + \nu) N_\psi\right] - w_o \cos \psi \tag{126}$$

The preceding equation for u was reported earlier, equation (44), as being the most suitable one for the computer program.

REFERENCES

1. A. E. H. Love, The Mathematical Theory of Elasticity, 4th ed, Cambridge University Press, 1927; 1st American Printing, Dover Publications, New York, 1944.

2. S. Timoshenko and J. N. Goodier, Theory of Elasticity, 2d ed, McGraw-Hill, New York, 1951.

3. S. Timoshenko and S. Woinowsky-Krieger, Theory of [illegible]es and Shells, McGraw-Hill, New York, 1959.

4. B. A. Boley and J. H. Weiner, Theory of Thermal [illegible]s, Wiley, New York, 1960.

5. W. Flugge, Stresses in Shells, Springer, Berlin, 1960.

6. E. T. McDowell and E. Sternberg, "Axisymmetric Thermal Stresses in a Spherical Shell of Arbitrary Thickness," Journal of Applied Mechanics, Vol. 24, No. 3, pp. 376-284, 1957.

7. C. H. Tsao, "Thermal Stresses in Long Cylindrical Shells", Trans. ASME, Vol. 81, Series E, pp. 147-148, 1959.

8. E. S. Barrekette, "Thermal Stresses in Beams", Trans. ASME, Vol. 82, Series E, pp. 465-473, 1960.

9. M. H. Bloom et al, Aerodynamic and Structural Analysis of Radome Shells, Vol. II Structural Analysis, WADD Technical Report 59-22, General Applied Science Laboratories, Inc., Wright Air Development Division, ARDC, USAF, Wright-Patterson Air Force Base, Ohio, 1961.

10. C. W. Lee, "A Theory for Thick-Walled Cylinders Under Axisymmetric Loading," Proceedings of the Fourth U.S. National Congress of Applied Mechanics, ASME, pp. 667-676, 1962.

11. N. J. Hoff and C. C. W. A. Madsen, "Buckling of a Thin-Walled Circular Cylindrical Shell Heated Along an Axial Strip," Trans. ASME, Vol. 86, Series E, pp. 253-258, 1964.

12. R. M. Rivello, Thermal Stress Analysis of Sandwich Cylinders, TG-721, JHU/APL, 1965.

13. G. Dailey, Numerical Solutions of Axisymmetric Thermal Stress Problems, TG-876, JHU/APL, 1966.

14. S. Y. Lu and L. K. Chang, "Thermal Buckling of Conical Shells", Vol. 5, No. 10, AIAA Journal, pp. 1877-1882, 1967.

15. L. B. Weckesser, R. H. Hallendorff, and R. P. Suess, Environmental Limitations of Alumina, Fused Silica and Pyroceram 9606 Radomes, TG-865, (Confidential), JHU/APL, 1967.

16. R. M. Rivello, Thermal Stresses in Finite Length Sandwich Cylinders, TG-903, JHU/APL, 1967.

17. R. O. Weiss, The Thermal Stresses in a Thick-Walled Cone by the Method of Finite Differences, TG-914, JHU/APL, 1967.

18. P. P. Bijlaard, R. J. Dohrmann, and J. M. Duke, "Thermal Stress Analysis of Non-Uniformly Heated Cylindrical Shells and Its Application to a Steam Generator Membrane Wall", Trans. ASME, Vol. 90, Series A, pp. 73-81, 1968.

19. M. B. Tate, Functionalization of Pyroceram 9606 Test Data for Radome Thermal-Stress Analysis, TG-980, JHU/APL, 1968.

20. _____, Air Properties and Flow Conditions Around the Nose of a Blunt Radome, TG-981, JHU/APL, 1968.

21. _____, Curvature Radii and Derivatives for Thermal-Stress Analysis of Von Karman Radomes, TG-982, JHU/APL, 1968.

22. _____, Statistical Analysis of Temperature Data from Wind Tunnel Test of a Von Karman Radome, TG-983, JHU/APL, 1968.

23. _____, Compound-Ogive Radomes as Substitute Structures for Von Karman Shapes, TG-985, JHU/APL, 1968.

24. _____, Approximate Functions as Particular Solutions in Thermal-Stress Analysis of an Ogival Radome, TG-1007, JHU/APL, 1968.

25. _____, Temperature Functions for Ogive-Radome Thermal-Stress Analysis, TG-1008, JHU/APL, 1968.

26. M. B. Tate, Solutions of Differential Equations for Thermal-Stress Analysis of an Ogival Radome, TG-1009, JHU/APL, 1968.

27. _____, Solutions of Differential Equations for Thermal-Stress Analysis of a Spherical Nosecap, TG-1070, JHU/APL, 1969.

INITIAL DISTRIBUTION EXTERNAL TO THE APPLIED PHYSICS LABORATORY*

The work reported in TG-1073 was done under Navy Contract NOw 62-0604-c. This work is related to Task A33, which is supported by Naval Ordnance Systems Command.

ORGANIZATION	LOCATION	ATTENTION	No. of Copies
DEPARTMENT OF DEFENSE			
DDC	Alexandria, Va.		20
DoD Director ate of Defense Research and Engineering	Washington, D. C.	Dr. Finn Larsen	1
Department of the Navy			
Headquarters			
NAVORDSYSCOM	Washington, D. C.	ORD-9132	2
		ORD-3511	1
NAVPLANTREPO	Silver Spring, Md.		1
Centers			
Naval Ship Research and Development Center	Annapolis, Md.	H. F. Koch	1
Laboratories			
NOL	White Oak, Md.	V. F. DeVost	1
		Dr. A. E. Seigel	1
		A. M. Corbin	1
		R. Mead	1
		G. Stathopoulos	1
		E. Rzepka	1
NRL	Washington, D. C.	R. E. Seely	1
Facility			
NOTS	China Lake, Calif.	W. J. Werback	1
Academy			
Naval Academy	Annapolis, Md.	Dr. E. O. Seaquist	1
U.S. GOVERNMENT AGENCIES			
National Aero. and Space Admin.			
Goddard Space Flight Center	Greenbelt, Md.	J. C. New	1
		J. Boeckle	1
		A. R. Timmons	1
Langley Aeronautical Laboratory	Langley Field, Va.	Mr. Paul Kuhn	1
		Dr. E. E. Lundquist	1
Library of Congress	Washington, D. C.	Dr. E. Wenk	1
UNIVERSITIES			
Iowa State Univ.,	Ames, Iowa	Dr. G. Murphy	1
		Dr. G. Town	1
Georgia Inst. of Tech.	Atlanta, Ga.	Dr. W. M. Sangster	1
Univ. of Missouri	Columbia, Mo.	Prof. K. H. Evans	1
		Dr. P. B. Burcham	1
		Prof. H. Rubey	1
Catholic Univ.	Washington, D. C.	Dean D. E. Marlowe	1

Requests for copies of this report from DoD activities and contractors should be directed to DDC, Cameron Station, Alexandria, Virginia 22314 using DDC Form 1 and, if necessary, DDC Form 55.

*Initial distribution of this document within the Applied Physics Laboratory has been made in accordance with a list on file in the APL Technical Reports Group.

INITIAL DISTRIBUTION EXTERNAL TO THE APPLIED PHYSICS LABORATORY*

ORGANIZATION	LOCATION	ATTENTION	No. of Copies
UNIVERSITIES (cont'd)			
Notre Dame Univ.	South Bend, Ind.	Dr. J. Hogat	1
Harvard Univ.	Cambridge, Mass.	Dr. B. Budiansky	1
Stanford Univ.	Palo Alto, Calif.	Dr. N. J. Hoff	1
Polytechnic Inst. of Brooklyn	Brooklyn, N. Y.	Dr. J. Kempner	1
		Dr. R. B. B. Moorman	1
Univ. of Buffalo	Buffalo, N. Y.	Dr. R. L. Kettner	1
Syracuse Univ.	Syracuse, N. Y.	Dr. C. Libove	1
Univ. of Massachusetts	Amherst, Mass.	Dr. W. A. Nash	1
Bradley Univ.	Peoria, Ill.	Dr. J. L. Jones	1
Illinois State Univ.	Charleston, Ill.	Dr. G. Q. Lefler	1
CONTRACTORS			
Bendix Missile Systems Div.	Mishawaka, Ind.	Dr. J. J. Toal, Dept. 838	1
McDonnell-Douglas Aircraft Corp.	St. Louis, Mo.	O. McBee	1
Ling-Temco-Vought, Aircraft and Missile Div.	Dallas, Texas	A. Murphy	1
Corning Glass Works	Corning, N. Y.	G. Tatnell	1
		R. Wasson	1
General Electric Co.	King of Prussia, Pa.	Space Sciences Lab.	1
Lockheed Aircraft Corp.	Burbank, Calif.	F. W. O'Green	1
Ingersoll-Rand Corp.	Bedminster, N. J.	Dr. W. W. Wise	1

*Initial distribution of this document within the Applied Physics Laboratory has been made in accordance with a list on file in the APL Technical Reports Group.

UNCLASSIFIED
Security Classification

DOCUMENT CONTROL DATA - R & D

Security classification of title, body of abstract and indexing annotation must be entered when the overall report is classified)

1 ORIGINATING ACTIVITY (Corporate author) The Johns Hopkins University Applied Physics Lab. 8621 Georgia Ave. Silver Spring, Md. 20910	2a. REPORT SECURITY CLASSIFICATION Unclassified 2b. GROUP

3 REPORT TITLE

Thermal Stresses in Ogival Radomes with Temperature-Dependent Material Properties

4 DESCRIPTIVE NOTES (Type of report and inclusive dates)

Technical Memorandum

5 AUTHOR(S) (First name, middle initial, last name)

Manford B. Tate

6 REPORT DATE	7a. TOTAL NO. OF PAGES	7b. NO OF REFS
July 1969	50	27

8a CONTRACT OR GRANT NO	9a. ORIGINATOR'S REPORT NUMBER(S)
NOw 62-0604-c b. PROJECT NO	TG-1073
c.	9b. OTHER REPORT NO(S) (Any other numbers that may be assigned this report)
d.	

10 DISTRIBUTION STATEMENT

This document has been approved for public release and sale; its distribution is unlimited.

11 SUPPLEMENTARY NOTES	12. SPONSORING MILITARY ACTIVITY
	Naval Ordnance Systems Command

13 ABSTRACT

The solution that is developed herein can be used to compute thermal stresses and displacements in the moderately thick walls of appreciably curved ogival shells whose material properties change with heat intensity along the span and through the wall. No restriction is placed on temperature dependent variations of the thermal stress expression.

Three examples of the computerized results are presented. The first example deals with a 28.3" x 6.75" bicentric-ogive radome; the second, with a thick-walled hemispheric radome; and the third, with a thin-walled hemisphere. In these calculations, linear spanwise temperature distributions are used that were obtained from experimental and heat-transfer analyses of a radome tested in a wind tunnel. Through the wall, over specified layers, the thermal-strain function is approximated as being linear with temperature. However, the temperature varies as a third-order nonlinear function through the thickness of the wall as found for the test radome. It appears that errors due to the approximation amount to less than four percent in general.

DD FORM 1 NOV 68 1473

UNCLASSIFIED
Security Classification

14. KEY WORDS

Thermal-stress analysis
Ogival Radome Thermal Stress
Temperature-dependent material properties